AEDC-TR-61-9

ay 1

DEVELOPMENT OF HYPERVELOCITY RANGE TECHNIQUES AT ARNOLD ENGINEERING DEVELOPMENT CENTER

By

J. Lukasiewicz, W. B. Stephenson,

P. L. Clemens, and D. E. Anderson

von Kármán Gas Dynamics Facility

ARO, Inc.

June 1961

ARNOLD ENGINEERING

DEVELOPMENT CENTER

AIR FORCE SYSTEMS COMMAND

US ★ AF

Additional copies of this report may be obtained from

ASTIA (TISVV)
ARLINGTON HALL STATION
ARLINGTON 12, VIRGINIA

note

Department of Defense contractors must be established for ASTIA services, or have their need-to-know certified by the cognizant military agency of their project or contract.

DEVELOPMENT OF HYPERVELOCITY RANGE TECHNIQUES
AT ARNOLD ENGINEERING DEVELOPMENT CENTER†

By

J. Lukasiewicz, W. B. Stephenson,
P. L. Clemens, and D. E. Anderson

VKF, ARO, Inc.

June 1961

Contract No. AF 40(600)-800 S/A 11(60-110)

ABSTRACT

Development of a hypervelocity launcher and range instrumentation in preparation for operation of a 1000-ft aeroballistic facility is described.

A method has been evolved for the gas-dynamics design of two-stage, light gas launchers. Performance, limitations, and mechanical design features of such launchers are discussed.

Instrumentation developments include: 1) projectile radiation actuated detector and spark trigger, 2) simple, Fresnel-lens shadowgraph performing satisfactorily at projectile speeds of 26,000 ft/sec, 3) telemeter capable of transmitting model pressure measurements at launch accelerations of 200,000 $\underline{g}$, 4) microwave velocity measuring technique.

CONTENTS

TABLE

ILLUSTRATIONS

NOMENCLATURE[†]

A	Cross-sectional area
a	Acoustic speed
C_1	Peak amplitude of detector output resulting from $TE_{1,1}$ mode reflectance, volts
C_2	Peak amplitude of detector output resulting from $TM_{0,1}$ mode reflectance, volts
C_3	Peak amplitude of detector output resulting from $TE_{2,1}$ mode reflectance, volts
D_1	Relative phase displacement of reflected $TE_{1,1}$ mode microwave energy, in.
D_2	Relative phase displacement of reflected $TM_{0,1}$ mode microwave energy, in.
D_3	Relative phase displacement of reflected $TE_{2,1}$ mode microwave energy, in.
e_0	Instantaneous detector output voltage, volts
g	Gravitational acceleration (approximately 32.2 ft/sec^2)
m_ℓ	Mass of projectile
m_p	Mass of piston
p	Pressure
s	Length
t	Time
u	Velocity
V_1	Volume of launcher high pressure chamber, in.^{3}
V_2	Volume V_1 plus volume of void separating projectile base from launcher diaphragm, in.^{3}
x	Coordinate along gun axis
α_1	Angular progression of $TE_{1,1}$ mode standing wave energy, radian/in.
α_2	Angular progression of $TM_{0,1}$ mode standing wave energy, radian/in.
α_3	Angular progression of $TE_{2,1}$ mode standing wave energy, radian/in.

[†]See also Fig. 5

γ — Ratio of specific heats

Δs_ℓ — Initial projectile motion

Δt_ℓ — Duration of initial projectile motion

ζ — Peak acceleration, ft/sec^2

$\bar{()}$ — Dimensionless quantity

$()_c$ — Chamber

$()_F$ — Front piston face

$()_f$ — Final state of second-stage propellant

$()_\ell$ — Launch tube

$()_p$ — Pump tube

$()_R$ — Rear piston face

DEVELOPMENT OF HYPERVELOCITY RANGE TECHNIQUES
AT ARNOLD ENGINEERING DEVELOPMENT CENTER [†]

By

J. Lukasiewicz[1], W. B. Stephenson[2],
P. L. Clemens[3], and D. E. Anderson[4]

ARO, Inc.

1. INTRODUCTION

The von Kármán Gas Dynamics Facility, one of the major laboratories at the Arnold Engineering Development Center (AEDC), Air Force Systems Command, USAF, is concerned with the investigation of flight at supersonic and hypersonic speeds. Conventional, low density, and hotshot-type wind tunnels provide simulation at velocities up to about 10,000 ft/sec, that is, at enthalpy levels at which real gas effects may be expected to be small. The main limitations of facilities of this general type are, on the one hand, the maximum conditions (enthalpy and density) which can be attained in the reservoir from which the working fluid is accelerated and, on the other hand, the freezing of flow during expansion from low reservoir densities.

Since, in principle, the aeroballistic range technique overcomes both of these difficulties, it was decided some time ago to augment the VKF spectrum of test units by the addition of a large aeroballistic range facility. The construction of this variable density, 1000-ft range started last year and is to be completed in 1962. Figure 1 shows a perspective view of the 1000-ft range now being built. The range tank, 1000 ft long and 10 ft in diameter, is entirely contained in a service tunnel, 20 ft wide by 14 ft high. The first 85 feet of the tank form the blast chamber. The initial launcher, shown in Fig. 2, will be of the two-stage, powder-He-H_2 type, with a 2.5-in.-diam launch tube. It is designed for 25,000 ft/sec velocity with a one-caliber, plastic projectile. The range will be instrumented with 43 orthogonal axes, Fresnel-shadowgraph and timing stations, one schlieren station, and a spark X-ray unit. Other instrumentation will include model telemetry, microwave velocity measuring techniques, radiation measurements and special systems for determination of drag at low densities.

[†]Paper presented at the ARPA-ARGMA-CARDE Symposium on Aeroballistic Ranges, Quebec, June 29-30, 1961

[1]Chief, von Kármán Gas Dynamics Facility

[2]Manager, Aeroballistic Branch, von Kármán Gas Dynamics Facility

[3]Supervisor, Instrumentation Development Section, von Kármán Gas Dynamics Facility

[4]Supervisor, Development Section, Aeroballistic Branch, von Kármán Gas Dynamics Facility

During the past three years, in preparation for operation of the new range, development of launcher and instrumentation has been underway in the VKF, and the results obtained to date are summarized here. This work is being done in pilot facilities, which include a 100-ft long, 6-ft diam, variable density range; a 140-ft long atmospheric range; and a number of launchers including a 40-mm, H_2-O_2-He NOL-type gun, a 0.5-in., two-stage, light gas gun, a 20-mm electric-arc gun, and a 40-mm cold gas gun.

2. LAUNCHER DEVELOPMENT

2.1 ELECTRIC-ARC-HEATED LAUNCHER EXPERIMENTS

The interest in launchers originated in VKF in connection with applications of electric-arc heating to hypervelocity test facilities. This technique resulted in the development of hotshot-type tunnels (Refs. 1,3) and was also applied to experimental launchers. Preliminary electric-gun experiments were made in 1953 using a small capacitor bank, Ref. 2. Later, a 10-megajoule, inductive storage, available for drive of a hotshot tunnel, was used to power a 20-mm launcher. With this gun, some 20 shots were fired which provided sufficient data for performance analysis. The maximum velocity obtained was about 13,000 ft/sec with a 4-gram projectile.

Figure 3 shows the construction of the launcher and Fig. 4 gives the results of analysis of experimental firings, which revealed the source of poor actual performance of the experimental electric gun. Three quantities are plotted in terms of the initial helium charge density:

a. the contaminant mass fraction $m_c/(m_c + m_{He})$, where m_c is the mass of materials lost from electrodes and other parts of the chamber during firing, and m_{He} is the mass of the propellant gas;

b. the ratio of actual projectile velocity u_{meas} to velocity $u_{m_c = 0}$ calculated for no contamination

c. the ratio of projectile velocity u_{m_c} calculated for the actual contamination to velocity $u_{m_c = 0}$ calculated for no contamination

In calculating the contaminant mass fraction and the corresponding projectile velocity, it has been assumed that all of the lost electrode and arc chamber materials evaporate to add to the molecular weight of the propellant.

The reference velocity $u_{m_c = 0}$ for $\rho/\rho_0 = 2500$ was obtained by charging the chamber with cold helium until the diaphragm ruptured, thus giving a point with no contamination present.

For given available energy and maximum pressure, the maximum propellant temperature decreases with increasing charge mass or density ρ/ρ_0. Hence, the quantity $m_c/(m_c + m_{He})$ is seen to decrease with ρ/ρ_0 increasing, Fig. 4.

The agreement in the two velocity ratios, Fig. 4, indicates that the poor performance of the electric gun can be attributed primarily to the contamination of the propellant with heavy vapors.

Also, it is interesting to note that the gas temperature of about 2000 °K, at $\rho/\rho_0 \approx 400$ atm, at which contamination effects appear to be negligible, is close to the melting point of steel and copper.

From the above limited experimental data and from more extensive results obtained with the hotshot tunnels, Ref. 3, it became apparent that contamination of propellant gas with electrode and chamber materials was a serious obstacle in the way of exploitation of the potential electric-gun performance. It was realized that the problem could be overcome only by a lengthy experimental development. Since, on the other hand, excellent results were being obtained with the two-stage, light gas launcher of Bioletti and Cunningham, Ref. 4, it was decided to develop this type of gun for the new 1000-ft range.

2.2 METHOD OF DESIGN OF A TWO-STAGE LAUNCHER

In order to design a launcher of a specified performance for the 1000-ft range, it was necessary to develop a method of design which would include effects of the important physical variables. This was done by, first, analysis of the ideal interior ballistics of the two-stage launcher; secondly, by consideration of important factors not included in the idealized treatment; and thirdly, by correlation of the empirical data available from firings of the NASA Ames Research Center and the AEDC guns. This design method is summarized below and has been outlined in detail in Refs. 5, 6, and 7.

2.2.1 Ideal Interior Ballistics

A two-stage launcher and its wave diagram and notation used below are shown schematically in Fig. 5a. The chamber, c, is separated from the pump tube, p, by a diaphragm and piston. The second-stage propellant (in the pump tube) is compressed by the piston and accelerates the projectile in the launch tube, ℓ, after a diaphragm (or shear disc) breaks at the projectile base.

AEDC-TR-61-9

Piston Velocity. In order to determine the final state of the second-stage propellant, and hence the motion of the projectile, it is first necessary to calculate the piston motion. In the simplest case, shown in Fig. 5a, the chamber is assumed to be of the same diameter as the pump tube (no chambrage) and of sufficient length to prevent interference of the reflected rarefaction wave with the piston motion. With these assumptions, the pressure on the rear piston face p_R is calculated from the simple expansion wave motion in terms of piston velocity u_p.

Next, it is assumed that at all times a normal shock precedes the piston in the pump tube. Hence, the front face piston pressure p_F is given in terms of u_p, by the normal shock equation.

The piston motion is then computed as

$$\bar{s}_p = \int_0^{\bar{u}_p} \frac{\bar{u}_p \, d\bar{u}_p}{\bar{p}_R - \bar{p}_F}$$

with

$$\bar{s}_p = \frac{p_c A_p s_p}{m_p a_c^2}$$

where

A_p = piston area

m_p = piston mass

s_p = length of pump tube

a_c = initial speed of sound in the chamber

$\bar{u}_p = u_p/a_c$

$\bar{p}_R = p_R/p_c$, $\bar{p}_F = p_F/p_c$

$\bar{p}_p = p_p/p_c$

Figure 6 shows the results of the above calculation for products of combustion of a mixture of hydrogen-oxygen-helium ($3H_2 + O_2 + 8He$) as the first-stage propellant and helium in the pump tube for various pump tube initial pressures $\bar{p}_p$ and with $a_p/a_c = 0.457$. The validity of this calculation was verified by experiments in which piston velocity was measured directly. In these tests, the launch tube was removed and a diaphragm retained the initial pressure in the pump tube. The velocity of the piston was measured on emergence from the pump tube into vacuum. Three of the typical experimental points from these measurements are shown in Fig. 6. As will be noted the experimental points agree well

with the curves computed under the assumptions noted earlier. Although chambrage would tend to increase piston velocity, it is probable that the effect of its omission is compensated by the finite chamber length. More refined calculations, which would take into account the chamber volume and which are similar to those described below for the projectile motion, could be made also in this case.

Compression of Second Stage Propellant. Having determined piston velocity, it is now possible to consider the final phase of compression of the second-stage propellant. This occurs as a result of reflection of the shock from the closed end of the pump tube. The first reflection results in state (3), Fig. 5a. Assuming that the piston velocity has not diminished, state (4) after the first reflection from the piston face can be calculated. As the shock continues to reflect, the acoustic speed continues to increase, the shock Mach number becomes progressively smaller, and the compression approaches an isentropic process. Moreover, as a result of deceleration of a finite mass piston, the shock weakens, thus ensuring an even more nearly isentropic compression.

To determine the final state of the second-stage propellant, it is assumed that:

a. the compression occurs as a result of three shock transits, from state (1) to (4), and is followed by isentropic compression to final state (f), and

b. the kinetic energy of the piston is equal to the change in internal energy from the rest state (3) to the final state (f).

Results of calculations outlined above are shown in Figs. 7a and b, in a generalized form. The final acoustic velocity a_f/a_p and final pressure p_f/p_p are given in terms of piston speed u_p/a_p and piston mass parameter $\bar{m}_p = m_p a_p^2/A_p s_p p_p$, where s_p = pump tube length. The mass parameter is actually proportional to the ratio of piston mass to pump tube charge mass. The figure was constructed for helium and hydrogen at T_p = 300 °K.

Projectile Velocity. The next and final step is the calculation of the projectile velocity. This is done assuming that the projectile starts accelerating only after the piston has come to rest and the second-stage propellant has reached its final state (f), Fig. 5a.

In order to take account of the final volume of the second-stage chamber (i.e., the volume of propellant in state (f)), the projectile velocity is computed using the method of characteristics, as outlined in detail in Ref. 6. Initial projectile motion is given by the chamber pressure p_f, the launch tube ahead of the projectile being assumed evacuated.

A typical characteristics network for helium second-stage propellant is shown in Fig. 8. The results of such computations, for chambrage

ratios A_p/A_ℓ = ∞, 4 and 1 and chamber lengths,

$$s_f = p_f A_\ell s_f/(m_p a_f^2) = ∞, 2, 1, 0.5, 0.25, 0.125$$

are shown in Fig. 9. It is interesting to note that the compensating effects of chambrage and chamber length result in nearly the same projectile velocity and distance (or time) for equal chamber volumes.

In Fig. 10, the above observation is used to provide a convenient summary of the results of characteristics calculations. Here the velocity is normalized by the ideal velocity u_o ($A_p = A_\ell$, $s_f = ∞$) for which an analytic solution is obtained, and is plotted against the ratio chamber volume/launch tube volume, for constant values of launch tube length $\bar{s}_\ell$ and for chambrage values of 4 and 1 (no chambrage). It is apparent that large chamber volumes required for smaller $\bar{s}_\ell$ are associated with large acoustic speed and hence rapid communication of the decaying chamber pressure to the projectile base.

Although the results shown in Fig. 10 were obtained for helium (γ = 1.66), comparison of results given in Ref. 8 at large values of V_f/V_ℓ (γ = 1.25 and 1.40) suggests that Fig. 10 may be used with satisfactory accuracy for hydrogen.

2.2.2 The Main Factors which May Reduce Performance

From the preceding, the projectile velocity can be computed for the following given conditions:

    a. initial state of the propellant in the chamber,

    b. piston mass,

    c. pump tube length and initial state of the propellant,

    d. projectile mass,

    e. launch tube geometry.

Systematic analyses of the effects of physical variables are possible by which the design of a launcher can be accomplished, limits of performance can be estimated, and correlation of experimental data can be made (Ref. 7). The velocity computed will be an ideal one based on several, already noted simplifications, which follow:

    1. The piston arrives at its final position and stays fixed near the end of the pump tube.

    2. The projectile stays fixed until the final pressure is attained in the pump tube.

    3. There is no heat transferred to the walls.

    4. The launch tube is evacuated and friction is negligible.

    5. In the hydrogen calculations, it is assumed that the expansion of the propellant is ideal, i.e., γ = 1.4.

<p style="text-align:center">14</p>

The effects of the violation of the assumptions 1 to 3 above, resulting in piston reversal, initial projectile motion, and heat losses, are discussed below.

Piston Reversal. If the piston is too light relative to the projectile, its reversal will adversely affect the driving pressure during the time the projectile is in the launch tube, as indicated in Fig. 5b. The dimensionless parameter:

$$\frac{m_p A_\ell}{m_\ell A_p}$$

where

m_p = piston mass

m_ℓ = projectile mass

A_ℓ = launch tube area

A_p = pump tube area

provides a correlation factor for the effect of the rate of pressure drop resulting from piston reversal. A lower limit is placed on piston mass or pump tube size for a given launch tube to render this effect negligible.

Initial Projectile Motion. Referring to Fig. 5b, it is seen that the projectile starts to move under the reflection pressure, p_3. A measure of the distance the projectile moves before the final pressure appears in the pump tube is the distance moved in the time interval between arrival of the first two shocks at the end of the pump tube. In the design of a launcher, the length of the pump tube is limited by a restriction on the allowable initial projectile motion.

Heat (Temperature) Loss. Loss of heat from the propellant gas will lower its acoustic speed (and therefore launch velocity) in two ways: 1) by reducing its temperature and 2) by contaminating the gas with a heavy element (iron vapor). This latter effect was very pronounced in the electric-arc launcher tests already discussed, Fig. 4.

2.2.3 Experimental Results Obtained with a 0.5-in.-diam, Two-Stage, Light Gas Launcher

The experimental program was directed toward determining the magnitude of corrections to the idealized interior ballistic treatment resulting from the above three effects. The other assumptions mentioned were not greatly at variance with the experimental test conditions; the launch tube had only 1 to 2 mm Hg air pressure, and helium was the propellant in most rounds. The effect of friction has not been well established; however, experience with various types of launchers indicates that it is small (Ref. 5).

A launcher, Fig. 11, was assembled using as the first stage a 40-mm, H_2-O_2-He configuration of NOL design. Pump tube lengths were 20.5 ft and 10.5 ft with a diameter of 1.58 in. Initially, a 20-mm launch tube liner was used; however, calculations of final volume indicated that the launch tube was too large. Therefore, 0.50-in.-bore, launch tubes 8 to 13 ft in length were used in all the tests. During the program of testing, preliminary, unpublished, hydrogen thermodynamic data became available from the Bureau of Standards, making it possible to compute launcher performance for this propellant. Much lower final temperatures resulted for hydrogen compared with helium, and it was found that the effect of final temperature in the pump tube could be isolated.

In Table 1, a series of rounds is listed in which most of the physical parameters of the launcher were varied. Measured launch velocities are compared with those computed to provide a basis for correlation. Piston velocities were calculated for the fraction of complete combustion determined from the measured combustion chamber pressure, p_c, by the method of Ref. 5. The initial projectile motion $(\Delta s_\ell/s_\ell)^\dagger$, piston reversal parameter $(m_p A_\ell)/(m_\ell A_p)$, and final temperature are tabulated in Table 1. Figure 12 shows the ratio of measured-to-calculated launch velocity as a function of each of these quantities.

Careful examination of the data reveals trends that are not superficially obvious.

Piston Reversal Correction. The group of rounds 140-143 had low values of the piston reversal parameter, as well as small values of the initial projectile motion parameter and of the final temperature. Therefore, this set of points was used (see also Ref. 7) to establish a piston reversal correction term, as follows:

$$\frac{u}{u_{calc}} = 1 - 0.4\left(\frac{m_p A_\ell}{m_\ell A_p}\right)^{-2}$$

Initial Projectile Motion Correction. Figure 12c indicates that all of the hydrogen rounds had relatively low values of temperature T_f; and since their piston reversal parameter was large, Fig. 12a, they were used to determine the following initial projectile motion correction:

$$\frac{u}{u_{calc}} = 1 - 7.4(\Delta s_\ell/s_\ell)^3$$

_____

†Once the piston velocity is determined, the pressure after the first reflected shock p_3 and the time between first and second shock arrival at the end of the pump tube, Δt_ℓ, can be calculated. The amount of projectile motion Δs_ℓ under the action of p_3 during Δt_ℓ is computed using the normal interior ballistics equations.

Temperature Loss Correction. The above corrections were applied to the remaining helium rounds, and the differences between these corrected and the measured values were used to establish the temperature loss correction, as follows:

$$\frac{u}{u_{calc}} = 1 - 3(T_f - 2000) \times 10^{-5} \qquad (T_f \text{ in } °K)$$

Complete Correction Formula. To obtain the complete formula, the above expressions are added:

$$\frac{u}{u_{calc}} = 1 - \frac{0.4}{[(m_p A_\ell)/(m_\ell A_p)]^2} - 7.4(\Delta s_\ell/s_\ell)^3 - 3(T_f - 2000) \times 10^{-5}$$

The above empirical formula is compared with the experimental results in Fig. 13. Lines of 10-percent deviation from the perfect correlation are given, indicating that most of the points fall within about 6 percent. There is a reasonable explanation for most of those points which show a large deviation from the correlation: 1) projectiles Nos. 142 and 143 were made of aluminum and had a shear-out strength which was appreciably higher than any of the other rounds, and consequently the initial projectile motion may thereby have been restricted; 2) No. 146 had a very high maximum pressure $(p_f > 300,000 \text{ psi})$, and the high-pressure seal failed tending to lower launch velocity; 3) No. 154 was the only round to have a plastic entrance to the launch tube, and it is believed that vaporization of this element contributed to low velocity; and 4) No. 156 is an anomaly in that the recorded chamber pressure (upon which the calculated piston velocity was based) indicated more pressure than would be provided by 100-percent combustion in a closed chamber. In calculating the velocity, 100-percent combustion was assumed. It is suspected that the transducer calibration was erroneous and that the calculated launch velocity was too high.

2.3 ACTUAL PERFORMANCE OF TWO-STAGE LAUNCHERS

The theoretical performance calculations modified by the empirical correlations given above provide a good estimate of the launch speeds for actual configurations. The limitations and methods of improving the two-stage launcher can be investigated systematically. As an example, Fig. 14 shows the ideal and corrected velocity for the VKF 0.5-in. launcher with helium and hydrogen as propellants at a chamber pressure of 20,000 psi. The possibility of preheating the helium charge appears promising from the ideal calculations; however, if the effect of heat transfer is included, the maximum launch velocity is only slightly greater at $p_f = 200,000$ psi.

Hydrogen is a much cooler propellant, and the correction for heat transfer is smaller so that the actual performance is close to the ideal,

as shown in Fig. 14. In order to obtain the potential high launch velocities using hydrogen, high final pressure must be provided for as shown. In fact, if the maximum pressure is 200,000 psi, almost the same launch velocity is obtained for helium and unheated hydrogen. By heating hydrogen to 600 °K, an increase of 3000 to 4000 ft/sec is expected.

The experience to date with plastic pistons has led to the tentative conclusion that lengths shorter than one caliber will not contain the high final pressures (200,000-300,000 psi). In theory, high piston speed is desirable to obtain the maximum launch velocity for a fixed final pressure. This condition obtains for a light piston and high chamber pressure; however, calculations (even neglecting the heat losses) show that the advantage of high piston velocity is small when the final pressure is fixed and that little improvement in launch velocity will result from doubling the chamber pressure or halving the piston mass. When the effect of high final temperature is introduced, the small favorable change in launch velocity with piston speed is attenuated or possibly reversed.

Figure 15 is the result of a study to determine an optimum pump tube size for a small terminal ballistics launcher with a 10-ft, 0.5-in. caliber launch tube. The final pressure in the pump tube was fixed at 350,000 psi, and the pump tube diameter and length were varied for several piston speeds. With an increase in pump tube length along any of the curves, the final temperature and initial projectile motion increase. The launch velocity therefore increases to a maximum, and then drops as a result of the corrections for projectile start and temperature. The reversal in the trend for $u_p/a_p = 1.8$ is attributed to the same cause.

Increasing piston velocity has two effects: 1) the final temperature is increased, and 2) projectile initial motion is decreased because of the shorter time between shock arrivals.

The effect of pump tube area, A_p, is to provide an increase in final volume to supply the launch tube. The launch velocity will approach an asymptote corresponding to an infinite volume ratio (final volume/launch tube volume). This effect is pronounced when the area is increased from 1 to 2 sq in., less from 2 to 4, and further increase in area will produce only a small increase in launch velocity.

Figure 15 shows that velocities more than slightly over 30,000 ft/sec are not likely to be attained with the conventional, two-stage launcher using unheated hydrogen and releasing the projectile at the incident shock arrival time. The pump tube length has little effect on launch velocity over a wide range — 6 to 20 ft in this case.

Improvements are possible by 1) retaining the projectile until the final pressure rise, 2) increasing maximum pressures beyond 350,000 psi, and 3) raising the pump tube charge temperature over 300 °K. There is some doubt that 1) or 2) can be accomplished without destroying the projectile. As for preheating the pump tube charge, experiments are now being conducted at the VKF to assess the magnitude of its effect.

18

2.4 MECHANICAL DESIGN FEATURES OF A TWO-STAGE LAUNCHER

To obtain ease and reliability of operation certain construction features have proved useful. Figure 11 is a layout of the 0.5-in. launcher mentioned above. Typical pressures through the gun with a 90-gram piston are 20,000 psi final pressure in the combustion chamber, 400 psi initial pressure in the pump tube, and 200,000 psi in the downstream end of high-pressure section. Corresponding maximum temperatures in the pump tube are 6000 °K if helium is used and 2000 °K for hydrogen. By suitable location of the seals with respect to the high-pressure section, maximum pressure which reaches any seal is held below 50,000 psi and no difficulty is experienced in seal failure.

For high-pressure section operation at pressures above 200,000 psi, a process of auto-frettage in place has been worked out which allows construction of very simple chambers which can withstand 350,000 psi. Figure 16 gives the internal pressure and plastic strain at the bore for a range of radius ratios when plastic flow has progressed to the outer wall (Ref. 9). The chamber is initially constructed of a monoblock cylinder (Fig. 17) with the inside diameter reduced near the launch tube end in accordance with the referenced plot and with some experimental information which shows the growth of chambers with respect to the final volume of compressed gas. The chamber is placed on the pump tube and the piston is fired with a heavy projectile until radial expansion in the high pressure region leaves the ID of the chamber uniform. Subsequent operation below the auto-frettage pressure is then elastic, allowing the application of strain gages to the outside of the chamber for the determination of chamber pressure.

Erosion of the launch tube is present to some extent in most of the shots, in particular those in which helium is used in the pump tube. To reduce costs of operation it is desirable to have low cost barrels, and to this end, it has been found that commercial tubing works quite well. A barrel is constructed of a support member around a piece of tubing whose ID is used as the launch tube. The tubing is either honed on the ID to the desired finish or a tungsten carbide ball is pushed down the barrel with two to three thousandths interference which produces a smooth surface. Total cost of a $\frac{1}{2}$ in. ID, 1 in. OD, tube liner is from $25 - $40 depending upon the amount of work required to finish the ID. It has been found that the outside diameter of the tube purchased from vendors will vary several thousandths, and it is desirable to specify a tolerance on the tube OD which is tighter than the normal MIL SPEC.

3. OPTICS

3.1 SHADOWGRAPH PERFORMANCE REQUIREMENTS

In the 1000-ft hypervelocity range now under construction in the von Kármán Gas Dynamics Facility, shadowgraphs are intended to provide only data describing projectile position and attitude. Optical information

regarding the nature of the flow field enveloping the projectile is to be obtained from a single, high speed schlieren system. Data relating to the composition and to the thermal excitation, both of the flow and of the ablation products which it may contain, are to be provided by spectrographs and monochromators. Although the performance requirements imposed upon the shadowgraphs have been described in Ref. 10, they are felt to be of sufficient importance to warrant their brief restatement here.

In addition to the usual criteria demanding brief (i.e., submicrosecond) exposure duration and large field of view, the shadowgraph system must fulfill several, more stringent requirements. The system must be impervious to the effects of the self-luminous shroud enveloping the projectile if other than the crudest attitude and position data are to evolve. If the use of a costly, ultra-high speed shuttering device (e.g., a Kerr cell or Faraday shutter) is to be avoided, then intensity of the flash source and efficiency of the optics must combine to "overpower" the effect of the self-luminosity of the projectile. Otherwise, a meaningless smear of light appears across the shadowgram masking whatever projectile image the light source might have made latent. Extremely intense flash sources tend inherently to be long duration sources. A good compromise here is not possible.

It is desirable that the bulk of the shadowgraph equipment, certainly the more expensive components, be located outside the range tank to reduce their vulnerability and to preclude the need for massive protective armor structures. Difficulty in insulating the high voltage wiring associated with the flash sources and in pressurizing "open" spark gaps is lessened if the flash apparatus is not enclosed in the evacuated tank. External mounting of cameras, flash sources, and associated apparatus also results in the more obvious advantage of their greater accessibility for maintenance. Location of the major optical elements outside the tank dictates the use either of very large windows or of re-focused or non-parallel shadowgraph rays, if a large field of view is to be covered. Cost of the optics is a factor favoring small ports and the use of re-focused or converging shadowgraph rays.

3.2 FRESNEL LENS SHADOWGRAPH

Promising shadowgraph results have been obtained in the 100-ft long, VKF pilot range using a direct, focused system as pictured in Fig. 18. Conical bundles of light rays, emerging from two spark sources, directly enter each of two, 15-in.-diam Fresnel lenses. Optical axes of these plastic Fresnel lenses and the axis of the range itself are mutually orthogonal. Two, 4-in. by 5-in. cameras provide the shadowgrams. The plane of focus for the camera lens-Fresnel lens combination falls at the

centerline of the range.[†] The shadowgram which results is a direct, back-lighted silhouette of the projectile. Surveyed fiducial indices are inscribed directly upon the plastic sheets which encase the Fresnel lens, and these markings appear in the shadowgram. The plastic Fresnel lens, although vulnerable, is inexpensive and is easily replaced in the event of damage. Although the optical quality of the Fresnel lens is not great, the aperture of the camera lens system is sufficiently large to accommodate the circle of confusion which the Fresnel lens imparts to the spark source image. As a result, little light is lost and optical efficiency is quite high. Resulting shadowgrams have adequately described projectile position and attitude. Figures 19a, b, and c are typical shadowgrams, accompanied by pertinent test data.

If the shadowgraph spark source is considered a true point source, the rays emerging from it are members of a conical system. The Fresnel lens shadowgraph, then, makes use of a simple, axisymmetric (rather than random) system of rays, and hyperfocal distances per se cannot be defined. However, the spark source diameter is finite, and the practical depth of field of the shadowgraph system is related to that diameter. Figure 20 illustrates this. For simplicity the camera optics and the Fresnel lens have, in Fig. 20, been consolidated into the single lens shown. It is assumed that this single lens does not aberrate. In Fig. 20a, classical ray tracing (Ref. 12) locates image M'-Q' of an object, M-Q, which lies in a plane containing the centerline of the hypervelocity range. However, the rays (1, 2, and 3) used in establishing the position of the image do not exist in the shadowgraph system inasmuch as none of them could have emanated from the point source, P_1, shown. Only those rays which are members of the conical system having its apex at the point source are available for image formation. Rays numbered 4 and 5 are typical.

Let it now be assumed that the "point" source of Fig. 20a has finite diameter. The effect is illustrated, greatly exaggerated, by translating the point source to a new location, P_2. Rays numbered 6 and 7, emanating from the displaced source P_2, are also brought to focus at image Q' of object Q. It is seen that the diameter of the source does not influence the quality of the shadowgram if the projectile trajectory is coincident with the range centerline.

Figure 20b illustrates the effect of displacement of the object from the plane upon which the lens system has been focused. Classical ray tracing now shows the image to fall forward of the film plane and a circle of confusion of diameter δ would appear in the photographic

[†]As is noted in Ref. 11, focusing a shadowgraph upon a plane containing aerodynamic striations has the effect of minimizing the appearance of those striations in the resulting shadowgram. However, the desire here is to produce a sharply defined image of the projectile itself; hence, the system is focused upon the trajectory axis, and data relating to the nature of the flow enveloping the model are sacrificed to ensure shadowgrams which satisfactorily resolve projectile attitude and position. Flow-related data are to be provided by other systems.

negative, were the rays 1, 2, and 3 available for image formation. Recall that only conically dispersed rays such as 4 and 5, departing from point source P_1, are to be considered. It is evident that, since such rays as 1, 2, and 3 are omitted from the system and cannot interfere, an unconfused image will again be outlined in the film plane. The simplicity of the system of rays provided by the point source has left the term "focus" bereft of meaning.

Again, consider the source diameter to be finite. Rays 6 and 7 emanating from the displaced point source P_2 indicate that a circle of confusion of diameter δ' will now accompany the film plane silhouette of each point along the object. Finite source diameter introduces penumbratic blurring only in the event the projectile departs from the plane of focus. The degree of blurring is a direct function of the diameter of the source and is related inversely both to the distance separating the projectile from the source and to the focal length of the optical system. (Aperture ratio of the lens and other relationships between dimensions of the optical system also affect the appearance of the penumbra, but a discussion of these influences is considered beyond the purpose of this paper.)

3.3 SPARK LIGHT SOURCE

The spark sources are of the capacitor discharge type. One such unit is seen partially disassembled in Fig. 21a and assembled in Fig. 21b. Circuitry used in this flash source is shown in Fig. 22. The source's arc discharge occurs at a hole of 0.030-in. diameter through the apex of a conical electrode. The output light pulse emerges from within the electrode cone. A barium-titanate capacitor of coaxial configuration and having a capacitance of 0.024 microfarads is discharged from a maximum potential of 6500 volts. This nominal half-joule discharge provides an effective exposure duration of 0.1 microseconds, as measured between the one-third amplitude ordinates along the intensity vs time characteristic. The source's conical main electrode is made of Mallory metal (90-tungsten, 6-copper, 4-nickel). As a result, electrode replacement has been minimized. After more than 200 full-energy discharges, electrode erosion is barely discernible. A stainless steel trigger electrode of 0.031-in. diameter protrudes through an insulator within the tip of the domed main electrode. Although this latter electrode is of brass, the relatively greater surface area which is available to support the arc lessons erosion here.

As the spark source circuit diagram (Fig. 22) indicates, a voltage output pulse is made available to be used in starting and stopping chronograph counters for measurement of projectile velocities.

It develops that spark source exposure duration is the most limiting factor affecting the resolution with which projectile position and attitude may be determined. During the one-tenth microsecond exposure duration of the spark source described here, the projectile will have moved some 0.036 inches at an assumed velocity of 30,000 ft/sec. Errors introduced

by aberrations within the optics, by grain structure of the film, and by the geometry of the system can all be shown to be less in magnitude.

3.4 SHADOWGRAPH CAMERAS AND FILTERS

The cameras which have been used in the hypervelocity pilot range shadowgraph work are 4 in. by 5 in. Speed Graphic units fitted with $f/2.8$ lenses of 85-mm focal length. Camera shutters are held open electrically by solenoids throughout the launching and flight of the projectile. Dense blue filters (Wratten No. 49 and Cinemoid No. 20) have been used effectively at the camera lenses to lessen the sensitivity of the film to the luminosity of the flow which envelops the projectile. This self-luminous glow tends toward the longer, visible and infra-red wavelengths. References 13, 14, and 15 show that little emission among the wavelengths shorter than 4000 Å resulted from a series of high velocity flights of aluminum projectiles through rarefied air. Reference 16 indicates a similar tendency on the part of high velocity magnesium and Ethocel projectiles to radiate predominately at wavelengths longer than 4000 Å. Conversely, the flash of light from the spark source is richly actinic. The shadowgram which appears as Fig. 23 was produced by a Fresnel lens shadowgraph without the benefit of the spectral selectivity afforded by the use of the blue filter. The glowing gas enveloping the projectile produced a smear which all but obscured the image of the projectile formed by the spark source. This shadowgram appears in contrast to the shadowgram of Fig. 19b which was made with the blue filter but under otherwise similar conditions.

3.5 FILM

Kodak Royal-X Pan film was used in making all of the blue-light shadowgrams shown in this report. Although this film is panchromatic, use of the blue filter renders it orthochromatic in its spectral response. The ASA emulsion rating for this film is 1250 and is marginal for satisfactory use in the shadowgraph application. However, 20-minute developing in FR Corporation, X-500 developer at 80 °F results in an increase in effective emulsion rating to a value far exceeding 10,000.

3.6 OPTICAL TRIGGER PERFORMANCE REQUIREMENTS

A hypervelocity range shadowgraph, regardless of the excellence of its optics, can be of no value unless its operation is synchronized to coincide with the arrival of the projectile within the field of view of its optics. Conventionally, the triggering of the shadowgraph light source is done by a photoelectric sensing element. In the usual arrangement, the photodetector and a source of illumination face one another from opposite sides of the range centerline. Passage of the opaque projectile between them partially obstructs the detector's view of the illuminated field and results in an electrical output pulse which is used to trigger the shadowgraph spark source. Assorted light screen triggers of this

type were tried in the VKF hypervelocity pilot range in a wide variety of configurations. Repeatability of the units was poor, becoming especially erratic for projectile velocities exceeding 8500 ft/sec.

Several intrinsic disadvantages of the illuminated-field trigger system are worth mentioning. Unless the light screen is formed of a collimated, multiple reflected beam to provide a high signal-to-noise ratio, whatever lamp may be used to illuminate the detector-viewed field must be excited from an electrical supply which is virtually ripple-free. Otherwise, variations in light output are mistaken for interruption by projectiles. Of course, the detection circuitry can be designed to ignore low frequency light ripple and sense only the sharp, projectile-produced pulse, but this introduces an undesirable circuit complication. Light from the trigger's source must be carefully confined by lenses or by baffling to prevent its fogging the film in the relatively long interval during which the camera shutters remain open. The projectile, although opaque, is partially surrounded by glowing gasses and is ill-suited for casting a shadow for detection by the photoelectric sensor. Furthermore the intensity of the gas luminosity is quite variable, depending upon velocity and the aerodynamic parameters, and thus a suitably intense light field for one shot may be less intense than the projectile itself for another. Increasing the intensity of the light field to accommodate all degrees of projectile luminosity saturates the photoelectric transducer leaving its sensitivity intolerably attenuated.

An examination of the performance desired of a shadowgraph trigger device is in order. The trigger must be impervious to the presence and to the intensity of the projectile's self-luminous envelopment. Bursts of extraneous illumination, as from the muzzle blast or from impingement of small particles upon range hardware, must not affect its operation. The trigger must be relatively free from microphonic interactions if it is not to be prematurely pulsed by the high velocity, blast-induced acoustical wave which is propagated through the range hardware. Trigger circuitry must not be susceptible to the extraneous electrical "noise" signals which are generated by the operation of other shadowgraphs. To eliminate time-delay circuitry from between the detector and the shadowgraph light source, it is desirable that the optical axis of the detector device and that of the shadowgraph coincide.

3.7 RADIATION DETECTOR

A projectile detector and shadowgraph triggering arrangement which meets the requirements outlined here has been developed in the VKF and is shown schematically in Fig. 18. Here, an optical cavity provides a dark field which is viewed by the detector unit. Baffling confines the field of view of the detector to the interior of the optical cavity. The optical cavity is formed within two, exponentially curved sheets of metal which are joined along a common seam and are closed at their ends. The interior of the cavity is coated with a dull, non-reflecting, black paint. The shape of the cavity ensures that no rays entering it can return to

the exterior. As the glowing projectile enters the detector's wedge-shaped field of view, the trigger circuitry pulses the shadowgraph light source, and the shadowgram image is recorded. The circuitry of the detector unit (Fig. 24) is transistorized throughout, and microphonic effects are thereby avoided. The circuit shown here has both stability and sensitivity which are improved significantly over those of the detector reported in Ref. 10. The General Transistor Corporation type 2N469A phototransistor used here has a light sensitivity rated at 7 to 14.9 microamperes per foot candle. The alpha cutoff frequency is near two megacycles and spectral response, normalized with respect to light intensity, shows a marked peak in the near infra-red region at a wavelength of some 15,000 Å. Response drops to 50-percent at about 8000 Å.

The effect of the optical cavity upon detector reliability has been examined rather simply. Several detectors have been installed with cavities omitted. These detectors view the darkened walls of the range tank itself. Insufficient data have been gathered to permit a thorough statistical treatment of the differences in performance between detectors with and without optical cavities. However, during a recent series of 37 consecutive projectile launchings, a typical cavity-equipped detector pre-fired only once, failed to fire once, and functioned properly during the other launchings. Its counterpart, without a cavity, pre-fired three times, failed to fire twice, fired late once, and correctly recognized all other passes. (The projectile trajectory, during the single late firing, fell outside the field of view of the detector unit.) The greater incidence of early triggering on the part of the detector without a cavity is attributable to the greater degree to which it may be affected by spark source flashes from shadowgraphs located farther uprange. (Pre-fires have been observed usually to coincide with spark discharges at preceding units.) More effective blackening of the tank walls opposite the detectors is expected to obviate need for the optical cavities.

Since the detector relies upon self-luminosity for its operation and since the luminous intensity diminishes with decreasing velocity and with decreasing ambient density, there will be a velocity-density profile at which the detector will fail. Figure 25, adapted from Ref. 17, shows energy radiated from the stagnation region as a function of ambient density and projectile velocity. Within the operating areas indicated, tests with the dark field, transistorized detector system have resulted in greater than 80-percent reliability.

Sufficient data have not yet been accumulated to completely describe the detector's limiting profile. However, the empirical data subtended by areas A and B in Fig. 25 may be extrapolated to predict detector performance in the case of the 1000-ft long, 10-ft diameter hypervelocity range G. With spectral distribution assumed constant, the detector is sensitive only to the total energy it receives. Therefore, a given detector should function equally well at any point along a given, constant power density contour in Fig. 25 if it be assumed that the projectiles viewed are of unchanging shape and size and that they are traversing trajectories at constant distances from the detector. Using this relationship,

applying the inverse square law to accommodate the increase in range tank diameter, and considering the size of the larger projectiles which are to be launched in the larger range, the contour of anticipated detector performance shown in Fig. 25 results.

A one-shot thyratron circuit is interposed between the detector and the shadowgraph spark source to prevent multiple triggering by the small bits of debris which sometimes follow the projectile. This monostable circuit is self-resetting after a five-second interval.

4. TELEMETRY

4.1 TELEMETRY SYSTEM REQUIREMENTS

To be useful in instrumenting models for tests in a hypervelocity range, a radio telemeter must fulfill certain minimum requirements. It must be capable of withstanding gross accelerations. Studies involving the 0.5-in. diameter, two-stage launcher have indicated that projectiles to be fired from the later 2.5-in. gun must survive peak launching accelerations as great as 2 to 4 x 10^6 g if they are to achieve muzzle velocities of 25,000 ft/sec.[†] Also imposing a demand upon the telemeter package structure is the requirement that, during its initial acceleration, the base of the projectile must withstand pressures as high as 200,000 psi.

The telemeter must be small enough to fit within the model structure without weakening it excessively. The models being used have a cylindrical shape 40 mm in diameter and are 40 mm to 60 mm in length. These models are of no particular aerodynamic interest but are of value in telemetry development because they are simply fabricated and require no sabots. Their size makes them suitable for use with the future VKF launchers.

The telemeter must be capable of accurately measuring and transmitting many of the parameters customarily measured in ordinary wind tunnel testing. Multi-channel telemetry of a family of such test variables from a single model is desirable inasmuch as data correlation would be facilitated and the number of firings necessary to complete a given test program would be reduced.

4.2 TELEMETRY DEVELOPMENT

A variety of test parameters has been considered for telemetering. Temperatures, heat transfer rates, angular and translational accelerations, and pressures all are sufficiently important to make telemetering them

---

[†]From the above considerations it is evident that the telemetry technique as now developed will be limited to use with projectile velocities substantially lower than 25,000 ft/sec.

worthwhile. To facilitate the evaluation of test results during the
early phases of development, it was considered desirable that the telem-
etered variable should be one which would lend itself well to static
calibration and also that it should be one for which in-flight, theoreti-
cal values might readily and accurately be determined. Of all variables
considered, stagnation pressure appeared most nearly to fulfill these
requirements.

Both amplitude and frequency modulation techniques have been con-
sidered in the development of telemetry circuits. The greater accuracy
afforded by frequency modulation systems and the greater ease with which
resulting data might be digitized have led to a concentration of effort
on the design of f-m circuitry. Both subcarrier and direct modulation
f-m telemeters have been developed and tested. Although the use of f-m
subcarriers affords multi-channel capability, the development effort has
not yet produced pressure transducers which are electrically well suited
to modulating subcarrier signals. As a result, success with subcarrier
telemeters has been very limited. Circuitry of a typical, direct modula-
tion, 150 mc, f-m telemeter, using a variable capacitance transducer, is
shown in Fig. 26. A photograph of such a unit, prior to final potting,
appears as Fig. 27. Reference 10 describes the telemeter packaging in
some detail.

A short launcher of smooth 40-mm bore which uses unheated air to
burst a diaphragm is used to accelerate telemetry models into a recovery
box. Telemetry circuit and construction techniques are first proven with
this cold gas gun and then tested with a combustion gun in the evacuable
pilot range. Although it is a low velocity launcher, the cold gas gun
is capable of applying a peak acceleration of some 400,000 g to a 90-gram
telemeter package. Data acquisition equipment accompanying both this cold
gas gun and the hypervelocity pilot range is shown in Fig. 28. The 138-ft
atmospheric range into which the cold gas gun fires is equipped with a
telemetry receiving antenna and terminates in a sawdust filled recovery
box. The short launcher barrel and the use of a cold gas propellant limit
projectile velocities, facilitating projectile recovery. Many projectiles
have been launched repeatedly.

Pressure telemeter development follows a five step course of evolu-
tion:

Step I   Individual telemeter circuit components, encapsulated with-
          in epoxy slugs, are subjected to statically applied stresses
          while functioning in telemeter circuits whose remaining
          components are undisturbed. The testing allows: selection
          of particular components least likely to be affected by
          strains imparted during launching; and, selection of the
          particular orientation, with respect to applied stress, for
          which each component realizes the least strain effect. Ob-
          servation of behavior of epoxies during this testing also
          permits selective elimination of those which perform badly.

balloon is sealed to a tube which passes through the wall of the cylinder. As the balloon is slowly inflated with air, the air which had occupied the cylinder is driven out through an exhaust vent. The balloon is shaped to conform to the interior contours of the sealed chamber. Once the balloon has been inflated to fill the entire cylinder, its mouth-tubulation is opened and helium is introduced to the chamber through the former exhaust vent. The balloon is slowly collapsed against the floor of the chamber. The sealed chamber is left filled with helium at atmospheric pressure. This mechanism provides a positive purge of the air from within the chamber, insuring against contamination of the helium.

Segments of 0.005-in.-diam exothermic wire (Pyrofuze Corporation, affiliate of Sigmund Cohn Corporation) are laid against the diaphragms at the ends of the chamber. As the projectile emerges from the barrel of the cold gas gun, it actuates a light screen detector which initiates the discharge of a group of capacitors through the exothermic wires. The exploding wires strip the tightly tensioned diaphragms from the ends of the cylinder. Some ten milliseconds are consumed in thus removing the dental dam diaphragms. As the projectile enters and leaves the calibration chamber, it encounters abrupt density discontinuities. An in-flight measurement of telemeter sensitivity results.

This system has three advantages over its predecessor (Refs. 10 and 19): 1) the positive purge precludes contamination of the helium and eliminates a source of calibration error which does not lend itself to theoretical correction, 2) the sealed chamber covers prevent the leaks which contributed to contamination at the ends of the cylinder, and 3) the speedy cover removal minimizes diffusion of the helium at the ends of the chamber prior to entry of the projectile. (The dental dam covers are stripped from the chamber ends within ten milliseconds. Cover removal by the method previously used required 200 milliseconds.)

4.4 RESULTS OF TELEMETRY TESTS

Reference 10 reported four to fifteen percent accuracies among pressure data recovered in flight from telemeters launched at peak accelerations of 125,000 g. Recent development work has produced telemeters capable of surviving peak launching accelerations nearly twice as great with little decrease in accuracy of data received. A typical pressure telemeter oscillogram is reproduced as Fig. 30. Peak acceleration here was 215,000 g. Figure 31, a comparison of telemetered with theoretical stagnation pressures, evolved from the oscillographic data of Fig. 30. The notchlike depression seen in the pressure data resulted from the use of the helium-filled calibration chamber. The telemetered data of Fig. 31 differ from the theoretical curve by some 18 percent of full-scale pressure. The amplitude of the excursion in telemetered pressure, corresponding to entrance of the projectile into the helium chamber, reveals that sensitivity of the telemeter in flight differed by 11.6 percent from that established during static calibration prior to launching.

Tests made with telemeters which did not contain transducers have shown them to function at accelerations up to 560,000 g. It is thus evident that, at present, the transducer is the most limiting single component within the pressure telemeter.

5. PROJECTILE ACCELERATION MEASUREMENTS

Until recently, values of peak acceleration experienced by projectiles within the launcher barrels had been computed (Ref. 19) using the expression:

$$\frac{\zeta}{g} = \left(\frac{p_c A_\ell}{g m_\ell}\right) \left(\frac{V_1}{V_2}\right)^\gamma \qquad\qquad \text{Eq. (1)}$$

This equation neglects the effects of leakage of the propellant gas from behind the projectile and it does not take into account the forces resulting from friction between barrel walls and the projectile. Neither of these effects is particularly amenable to numerical analysis. Equation (1) assumes a purely adiabatic expansion of the propellant gas into the void separating the opened diaphragm from the base of the projectile; the process is, in fact, polytropic. The accuracy with which Eq. (1) produced values of peak acceleration was a matter of speculation, and direct measurements were desirable.

A microwave reflectometer has been devised and appears schematically as Fig. 32. This apparatus, modeled after the work of Pennelegion (Ref. 20), produces direct, time resolved recordings of the position of the projectile in the launcher barrel. Although its application has been limited to the cold gas gun which is used in the development of telemeters, the technique is adaptable to projectile position measurements in virtually any launcher. As shown in Fig. 32, a klystron operating in the X band (8.2 to 12.4 kmc) drives a loop probe which has been fitted into a recess near the muzzle of the launcher barrel. The probe does not protrude into the barrel itself; hence, it neither interferes with nor is it damaged by the moving projectile. The launcher barrel behaves as a resonating, circular waveguide. The foreface of the projectile approximates a mismatched, reflecting termination.

A portion of the microwave energy which negotiates the directional coupler in the forward direction is arrested by a non-reflecting termination impedance. The remainder is coupled to the barrel of the launcher, where it induces standing waves in various transverse electric and magnetic modes. Standing wave amplitude at the loop probe is a function of the frequency, the intensity and the mode of excitation, and the effective length of the barrel. Thus, for a given frequency and a single mode of constant amplitude excitation, the standing wave amplitude which is reflected to the crystal detector is related directly to the position of the projectile in the barrel. An oscillograph or magnetic tape recording of the output of the detector produces a time history of the position of the projectile.

Figure 33 reproduces a time-resolved record of projectile position which resulted from a typical launching. The reflectometer system had been statically calibrated, and it had been established that 2.06 inches of projectile travel shifted the train of standing waves through a single cycle. Harmonic content evident in the waveform seen in Fig. 33 is attributable to excitation of the launcher barrel in extraneous modes whose wavelengths in the barrel differ from that of the predominant $TE_{1,1}$ mode. The forcing frequency of nine kilomegacycles used here also excited the $TM_{0,1}$ and $TE_{2,1}$ modes. If reflectance of the projectile is taken as unity, an expression for the resultant detector output voltage as a function of the position of the projectile might be written:

$$e_0 = \left| C_1 \sin \alpha_1 \left(x_\ell + D_1 \right) + C_2 \sin \alpha_2 \left(x_\ell + D_2 \right) + C_3 \sin \alpha_3 \left(x_\ell + D_3 \right) \right|$$

Eq. (2)

References 21 and 22 enable evaluation of the wavelength constants of Eq. (2) for the extraneous modes in terms of the constant for the dominant mode:

$$\alpha_2 = 0.88 \, \alpha_1$$

and

$$\alpha_3 = 0.665 \, \alpha_1$$

As the wavelength of a particular mode increases, it more nearly approaches the wavelength unique for cutoff. The amplitudes of the three modes which are present therefore diminish progressively:

$$C_1 > C_2 > C_3$$

The projectile displacement data derived from Fig. 33 have been plotted and appear as Fig. 34. As computed from these data, the maximum velocity attained by the projectile was 2040 ft/sec. The average acceleration, occurring during the initial 375 microseconds of projectile motion, was 171,000 g. For this same launching, the value of peak acceleration given by Eq. (1) was 178,000 g. Disparity between the two methods, in this case, is 4.1 percent.

It is evident that for increased accuracy by the microwave reflectometer method the initial period of projectile motion must be scrutinized carefully. Work must be undertaken to provide microwave excitation in such a dominant mode and at such a frequency as will substantially shorten the wavelength of the standing wave system within the launcher barrel. A proportional increase in resolution should result. Efforts also must be made to eliminate from the barrel standing waves of extraneous modes which might introduce ambiguities among the data describing projectile position.

. 6. CONCLUSIONS

The work here described has, to date, resulted in the following satisfactory developments:

1. A rational gas-dynamics method of two-stage, light gas launcher design, based on idealized theory and experimental corrections;

2. Advantageous mechanical design procedures, including in-place auto-frettaging of high-pressure sections and economical launch tube liner fabrication;

3. Economical detector-shadowgraph system proven at speeds up to 26,000 ft/sec;

4. Telemeters capable of transmitting model pressures at launch accelerations of 200,000 $\underline{g}$;

5. A microwave technique of measurement of projectile velocity.

Future work is directed towards extension of the above techniques to higher velocities and development of instrumentation for measurement of physical properties of flow fields at extreme model speeds and model drag at low densities.

7. REFERENCES

1. Perry, R. W. and MacDermott, W. N. "Development of the Spark-Heated, Hypervelocity, Blowdown Tunnel - Hotshot." AEDC-TR-58-6, July 1958.

2. Bloxsom, D. E. "Production of High Temperature, Moderate Pressure Gases by Means of Electrical Spark Discharges." AEDC-TN-56-17, November 1956.

3. Lukasiewicz, J., Jackson, R., and van der Bliek, J. "Development of Capacitance- and Inductance-Driven Hotshot Tunnels." AEDC-TN-60-222, January 1961.

4. Bioletti, C. and Cunningham, B. E. "A High Velocity Gun Employing a Shock Compressed Light Gas." NASA-TN-D-307, February 1960.

5. Lord, M. E. "Performance of a 40-mm, Combustion Heated, Light Gas Gun Launcher." AEDC-TN-60-176, October 1960.

6. Stephenson, W. B. "Theoretical Light Gas Gun Performance." AEDC-TR-61-1, May 1961.

7. Stephenson, W. B. and Anderson, D. E. "Design of a Large, Two-Stage, Light-Gas Model Launcher." AEDC-TR-61-6, May 1961.

8. Seigel, A. E. and Dawson, V. C. D. "Results of Chambrage Experiments on Guns with Effectively Infinite Length Chambers." NAVORD Rept. 3636, U. S. Naval Ordnance Laboratory, April 1954.

9. Faupel, J. H. and Furbeck, A. R. "Influence of Residual Stress on Behavior of Thick-Wall and Closed-End Cylinders." ASME Transactions, Vol. 75, No. 3, April 1953, p. 345.

10. Clemens, P. L. and Kingery, M. K. "Development of Instrumentation for a Hypervelocity Range." AEDC-TN-60-230, December 1960. (Paper delivered at the IAS-sponsored National Symposium on Hypervelocity Techniques, Denver, Colorado, October 20, 1960.)

11. Dean, Robert C., Jr. (editor). "Aerodynamic Measurements." Gas Turbine Laboratory, Massachusetts Institute of Technology, 1953.

12. Jenkins, Francis A. and White, Harvey, E. Fundamentals of Optics. McGraw-Hill Book Company, New York, 1957.

13. Bull, G. V. "Re-Entry Studies in Free Flight Ranges." IAS Paper No. 59-143. (Presented at the Seventh Anglo-American Aeronautical Conference, New York, October 5, 1959.)

14. St. Pierre, C. "The Visible Emission from $\frac{1}{2}$-inch Hypervelocity Models Measured with a Moving Target Monochromator." CARDE-TM-AB-59, May 1960.

15. St. Pierre, C. "Emitted Radiation Studies Performed in a Hypersonic Range with Half-Inch Models." CARDE-TM-AB-52, May 1960.

16. Liu, I. D. "Spectra Associated with High Speed Projectiles Obtained with a Large Aperture Streak Spectrograph." CARDE-TM-AB-68, January 1961.

17. Kivell, Bennett. "Radiation from Hot Air and Stagnation Heating." AVCO Research Report No. 79, AFBMD-TR-59-20, October 1959.

18. Kingery, M. K. and Clemens, P. L. "An Assessment of Readout Errors Encountered in Radio Telemetry from Gun-Launched Hypervelocity Projectiles." AEDC-TN-61-58, May 1961.

19. Kingery, M. K., Choate, R. H., and Young, R. P. "Progress Report on Development of Telemetry for a Hypervelocity Range." AEDC-TN-60-214, December 1960.

20. Pennelegion, L. "Instrumentation of the University of Southampton Gun Tunnel." (thesis) University of Southampton, England, May 1959.

21. Markuvitz, N. (editor). Waveguide Handbook. (MIT Radiation Laboratory Series, Vol. 10). McGraw-Hill Book Company, New York, 1951.

22. Westman, H. P. (editor). "Reference Data for Radio Engineers." (Fourth Edition). International Telephone and Telegraph Corporation.

TABLE 1

EXPERIMENTAL RESULTS FROM 0.5-INCH DIAM TWO-STAGE LAUNCHER
Helium and Hydrogen Second Stage Propellants

Round	s_p ft	s_ℓ ft	m_p gram	m_ℓ gram	p_c psi	p_p psia	u_{meas} ft/sec	$\dfrac{u_{meas}}{u_{calc}}$	$\dfrac{\Delta s_\ell}{s_\ell}$	$\dfrac{m_p A_\ell}{m_\ell A_p}$	T_f °K
140 (He)	20.5	13.0	45.05	3.50	21,000	200	11,800	0.681	0.117	1.33	5,100
141	20.5	13.0	44.15	3.00	22,000	200	12,200	0.826	0.097	1.51	3,500
142	20.5	9.1	60.00	3.00	20,000	200	14,400	0.830	0.194	2.06	5,140
143	20.5	9.1	44.19	3.00	20,000	200	14,500	0.910	0.193	1.52	4,660
144	20.5	9.1	87.60	1.80	24,000	200	17,000	0.681	0.279	5.02	7,240
145	20.5	9.1	87.64	1.75	24,000	200	16,100	0.653	0.289	5.16	7,020
146	20.5	9.1	87.06	1.30	26,000	100	18,400	0.504	0.208	6.90	14,300
147	20.5	9.1	87.18	1.50	26,000	150	18,000	0.586	0.261	5.99	10,300
148	20.5	8.54	87.22	1.50	23,000	150	18,100	0.627	0.280	5.99	9,400
149	20.5	9.31	87.55	1.50	23,000	150	18,500	0.634	0.254	6.02	9,400
150	20.5	8.57	87.57	1.50	25,000	150	17,400	0.593	0.270	6.02	9,660
151	10.5	9.38	87.72	1.50	20,000	250	19,300	0.799	0.147	6.13	5,970
160	10.5	9.60	87.50	1.00	23,000	225	23,500	0.810	0.167	9.02	7,170
169	10.5	9.83	86.53	2.00	16,000	250	18,350	0.950	0.071	4.46	4,410
153 (H₂)	10.5	8.77	88.13	1.00	21,100	300	26,700	0.960	0.124	9.42	2,880
154	10.5	8.33	87.79	1.00	17,600	450	18,100	0.739	0.228	9.05	1,890
155	10.5	10.08	86.83	1.00	22,600	450	22,380	0.812	0.252	8.95	2,320
156	10.5	8.89	80.27	1.00	25,800	450	20,700	0.695	0.279	8.27	2,480
157	10.5	8.89	82.43	1.00	24,600	450	25,380	0.866	0.279	8.50	2,440
158	10.5	8.89	78.47	1.00	21,600	450	26,650	0.978	0.193	8.09	2,190
159	10.5	8.89	88.71	1.00	21,000	450	26,000	0.931	0.232	9.14	2,220
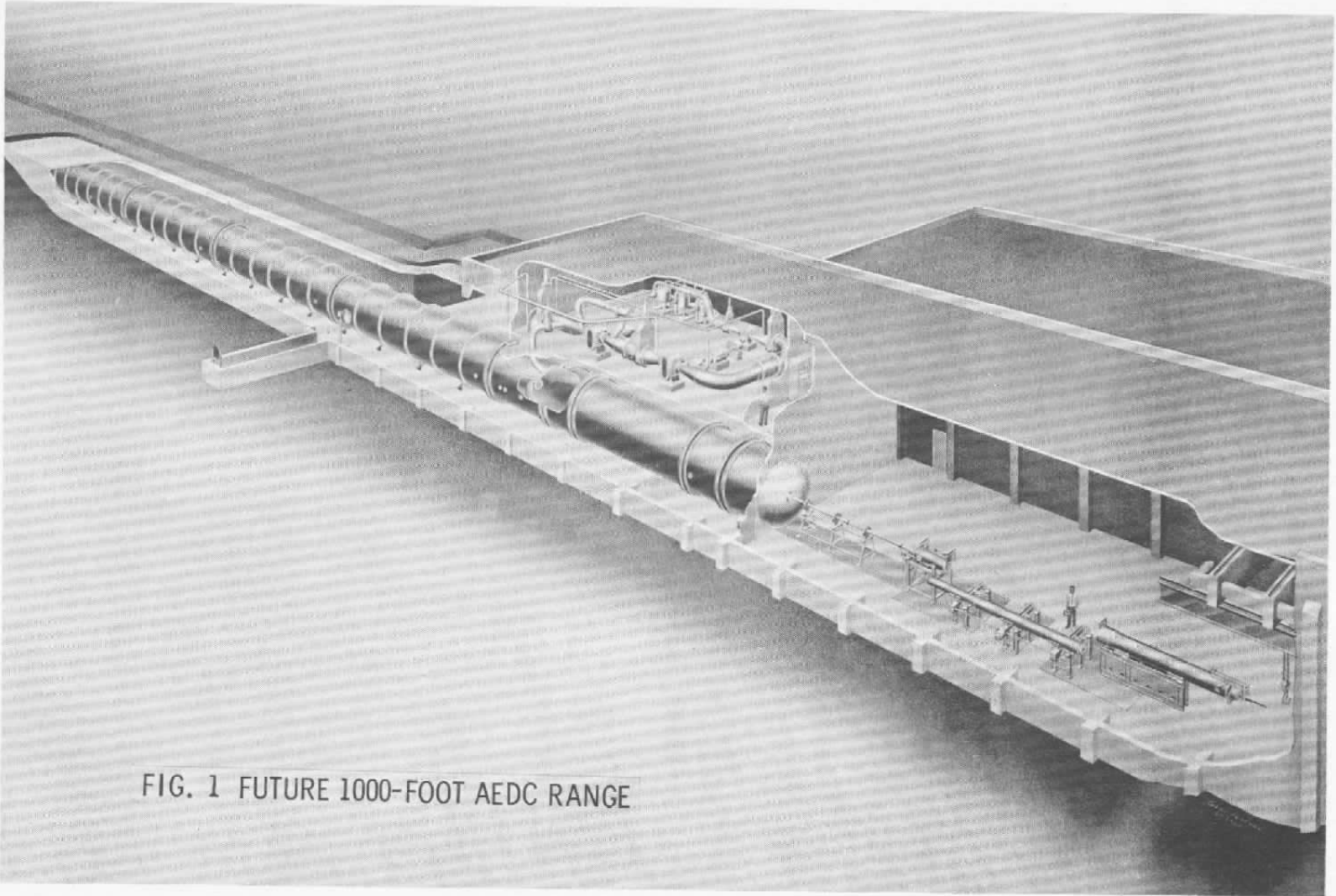
FIG. 1 FUTURE 1000-FOOT AEDC RANGE

37

AEDC-TR-61-9
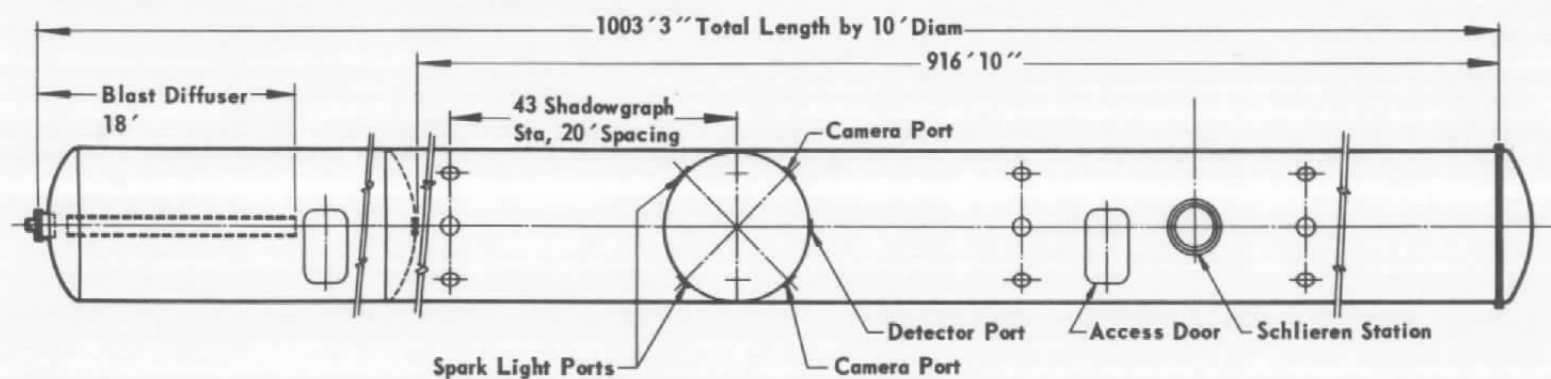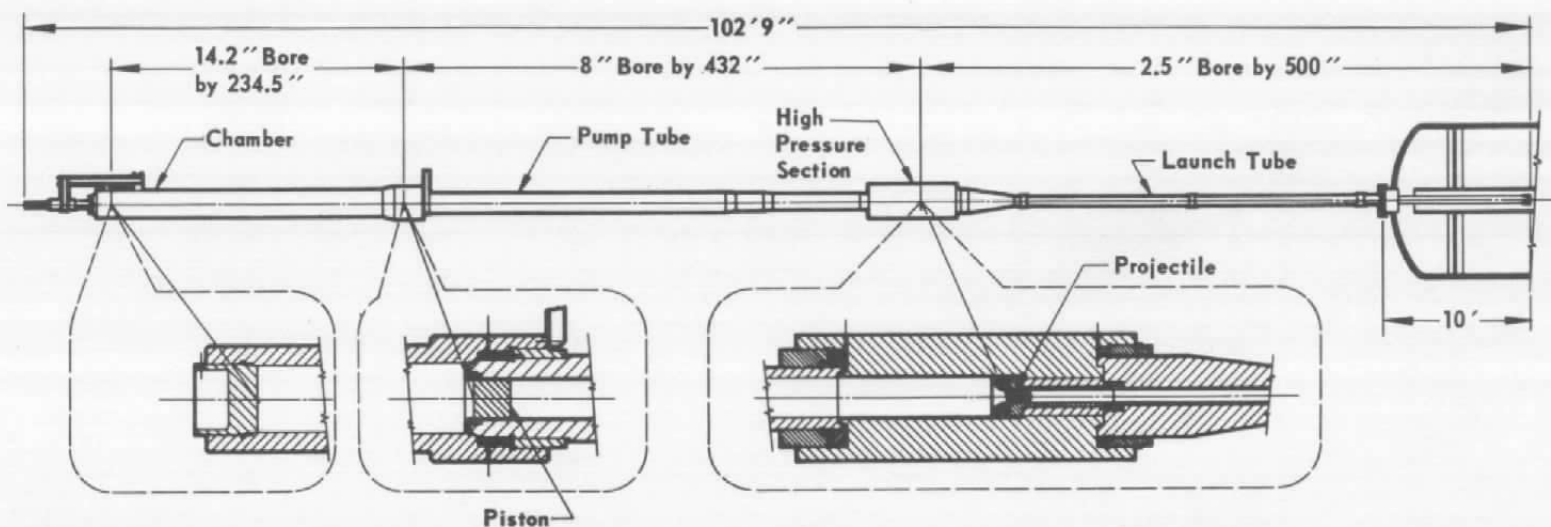
Fig. 2 2.5-Inch Diameter Launcher and Range Tank

PRESSURE VESSEL, 13 IN. OD

LINER

INNER LINER (PLASTIC OR COPPER), 5 IN. ID

NOSE BLOCK

SEAL

INSULATORS

LAUNCH TUBE, 2.5 IN. OD - 0.79 IN. (20 mm) ID

PROJECTILE AND SABOT

DIAPHRAGM

ARC

ENTRANCE PIECE

BREECH PLUG
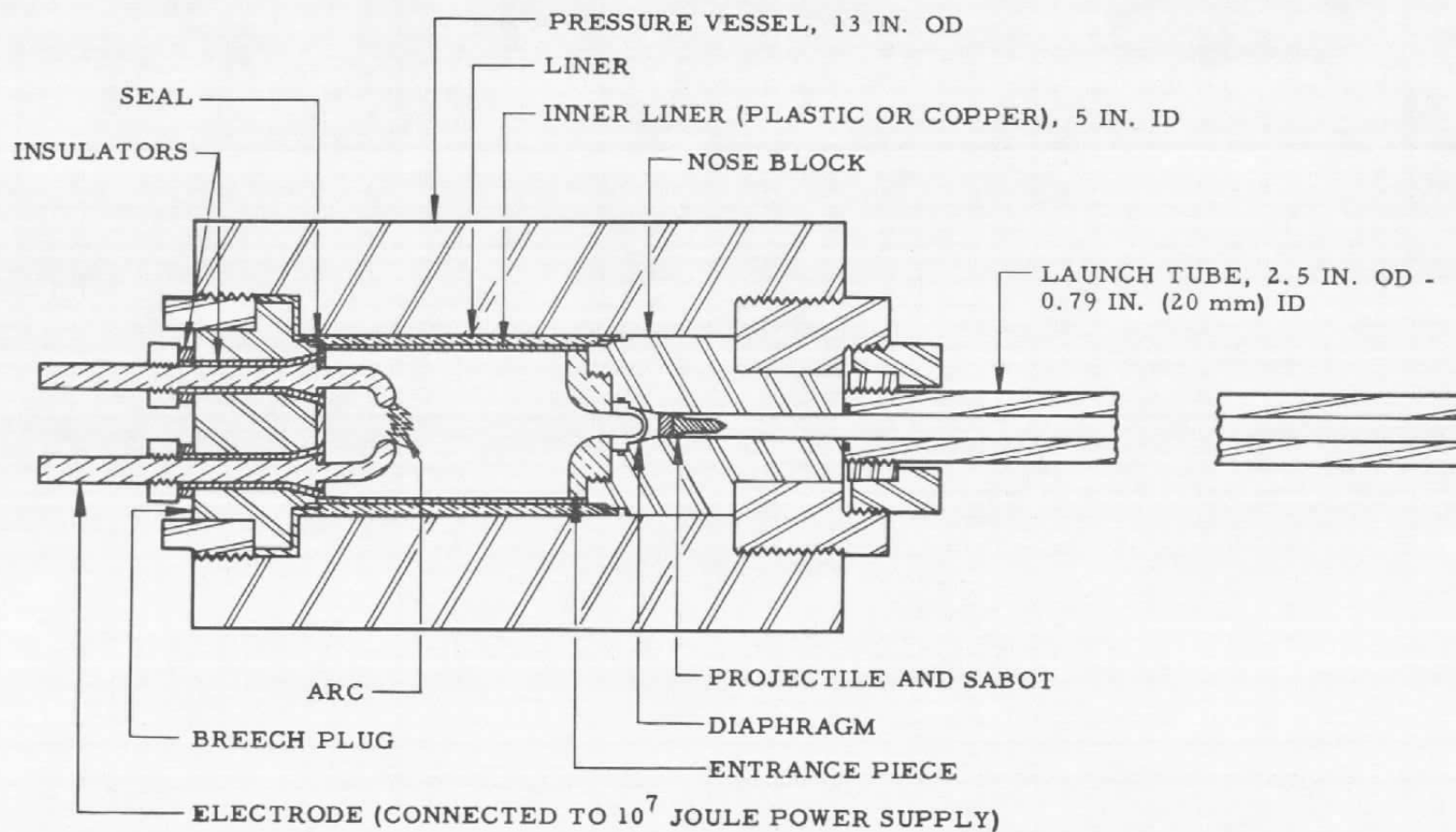
ELECTRODE (CONNECTED TO 10^7 JOULE POWER SUPPLY)

Fig. 3 Arc-Heated 20-mm Launcher
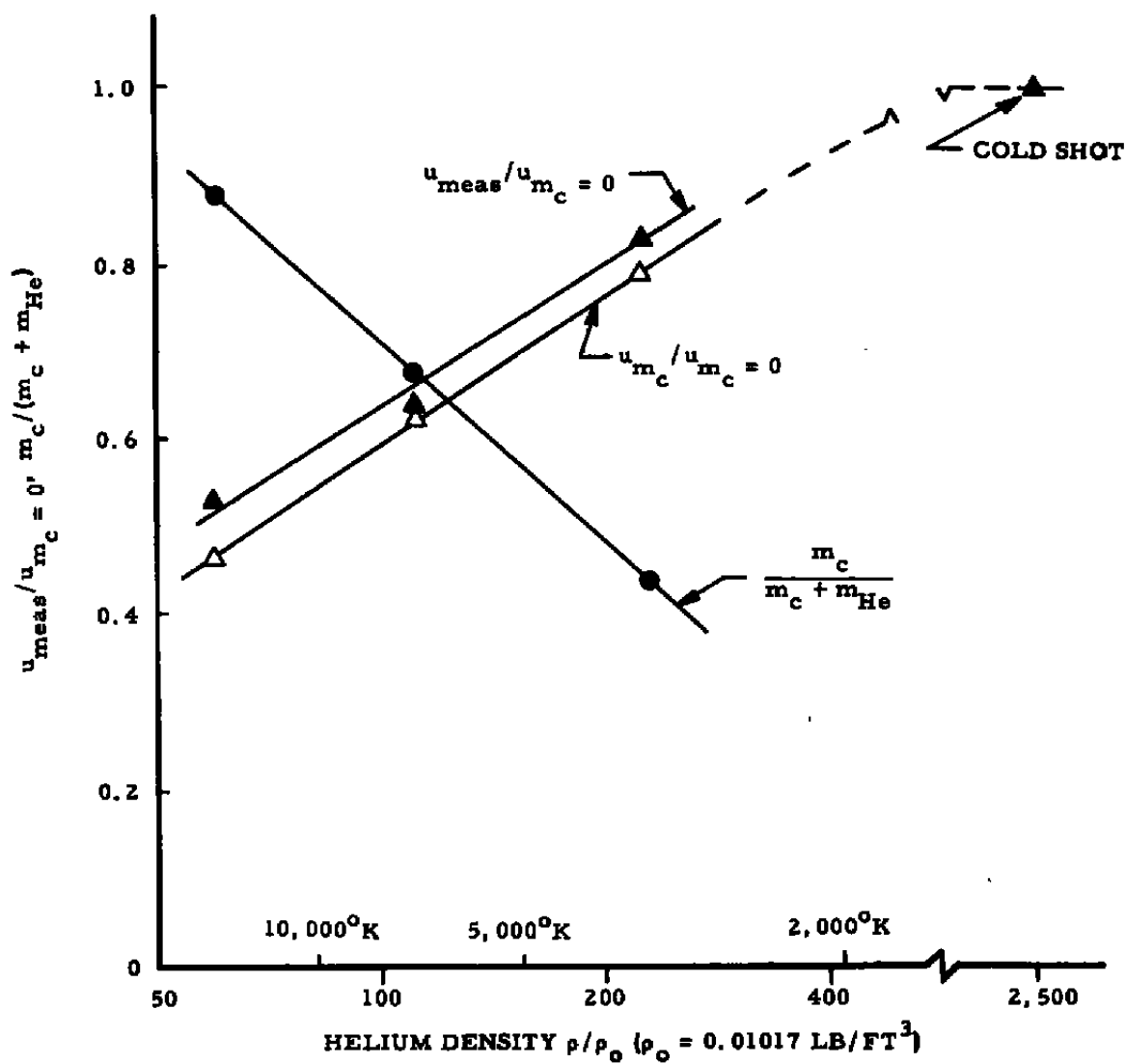
Fig. 4 Propellant Contamination and Its Effect on Projectile
Velocity (20-mm Electric Launcher)
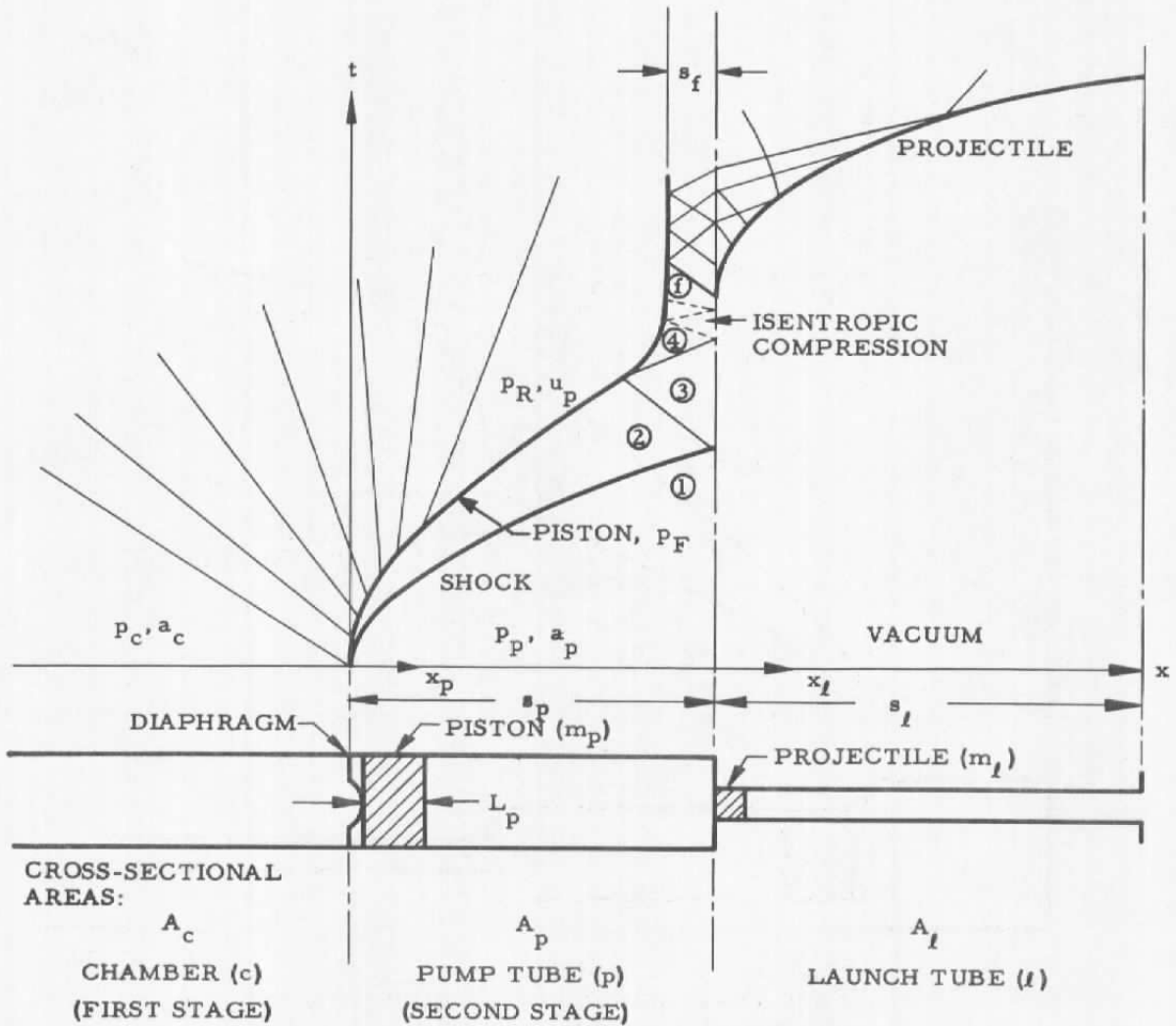
a. Idealized Model for Computation of Projectile Velocity

Fig. 5 Wave Diagrams of a Two-Stage Launcher
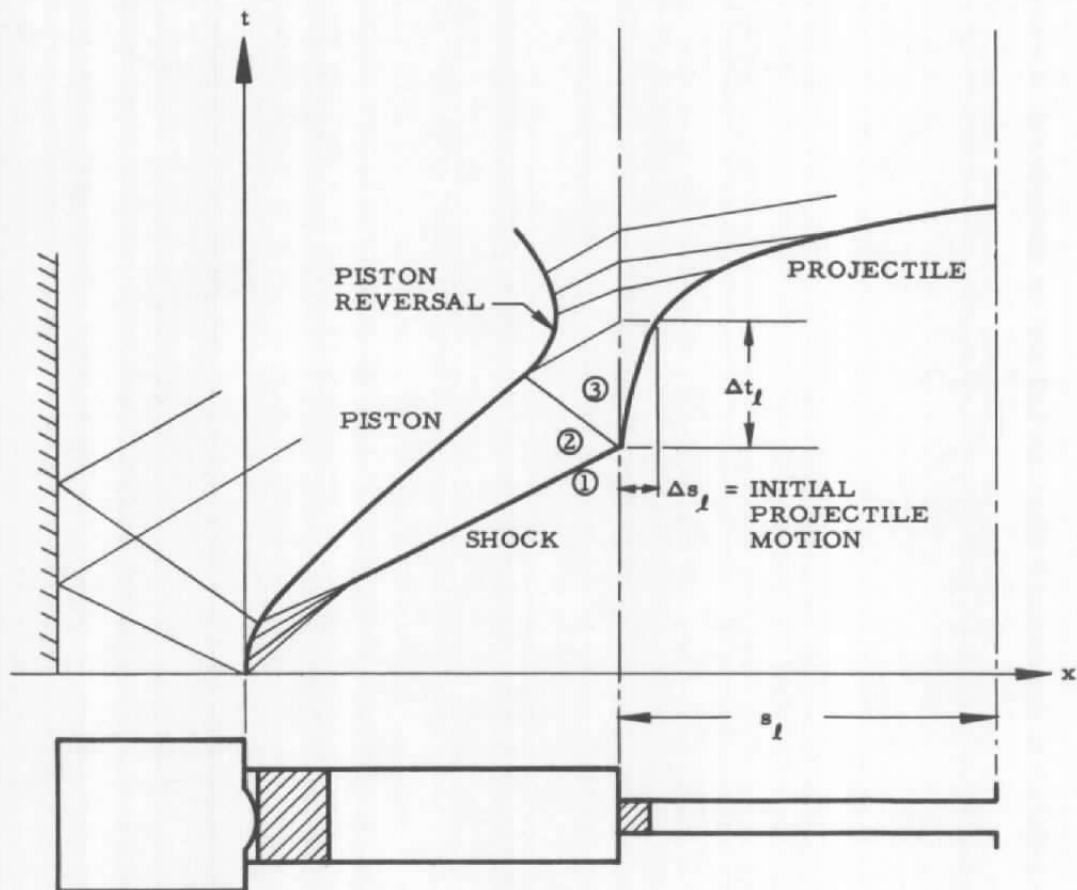
b. Wave Diagram Showing Piston Reversal
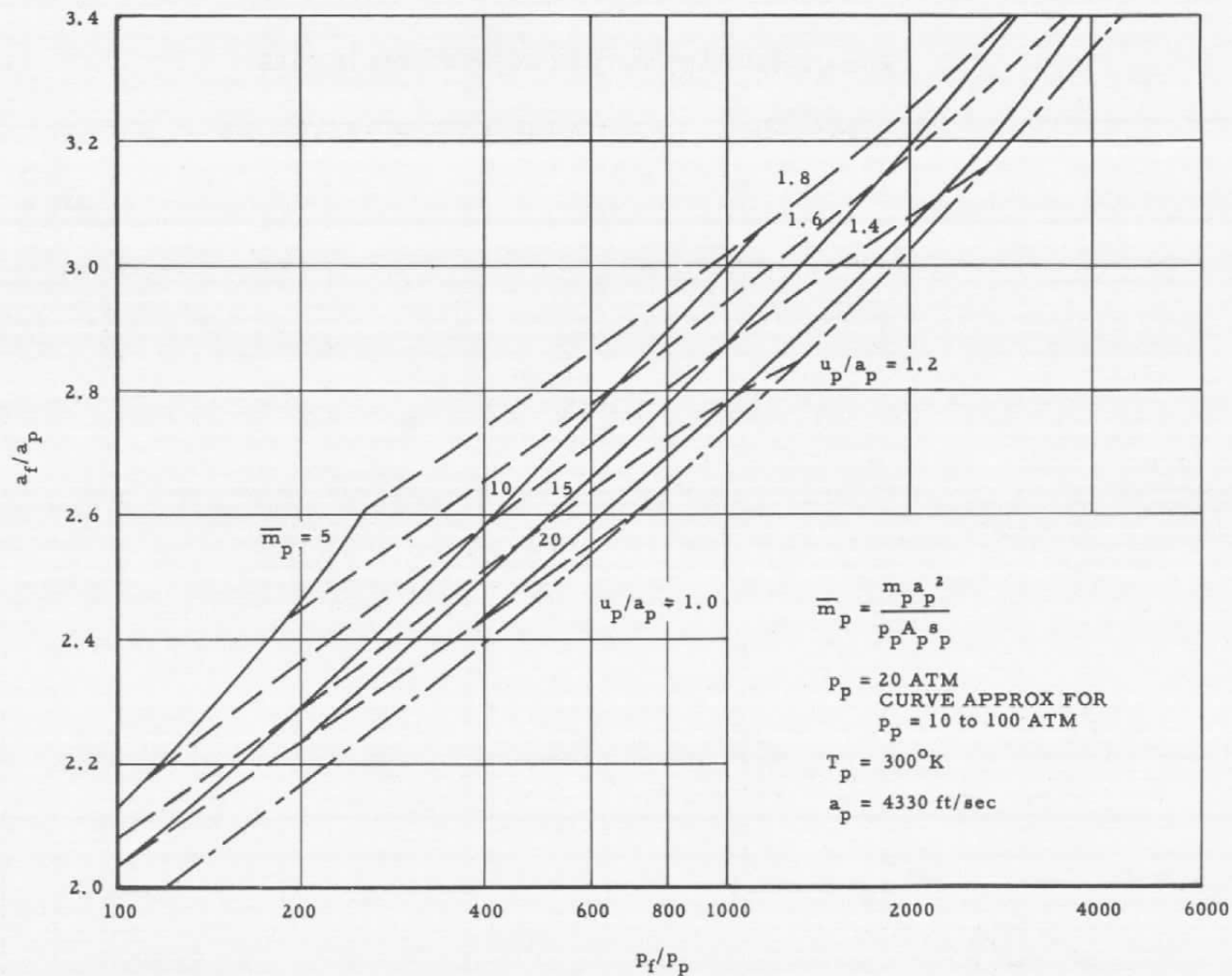and Initial Projectile Motion

Fig. 5 Concluded

Fig. 6 Piston Motion

The figure shows a plot with vertical axis labeled a_f/a_p ranging from 0 to 30, and horizontal axis labeled P_f/P_p ranging from 10 to 10^6 on a logarithmic scale. Curves are labeled with values $\overline{m}_p = 1$, 10, 20, 50, 100. Dashed curves are labeled $u_p/a_p = 1$, $u_p/a_p = 2$, 3, 4_s, and "Isentropic".

Annotations on the figure:

$$\overline{m}_p = \frac{m_p a_p^{\,2}}{p_p A_p s_p}$$

$\gamma = 1.66$

$T_p = 300°K$

$a_p = 3320 \text{ ft/sec}$
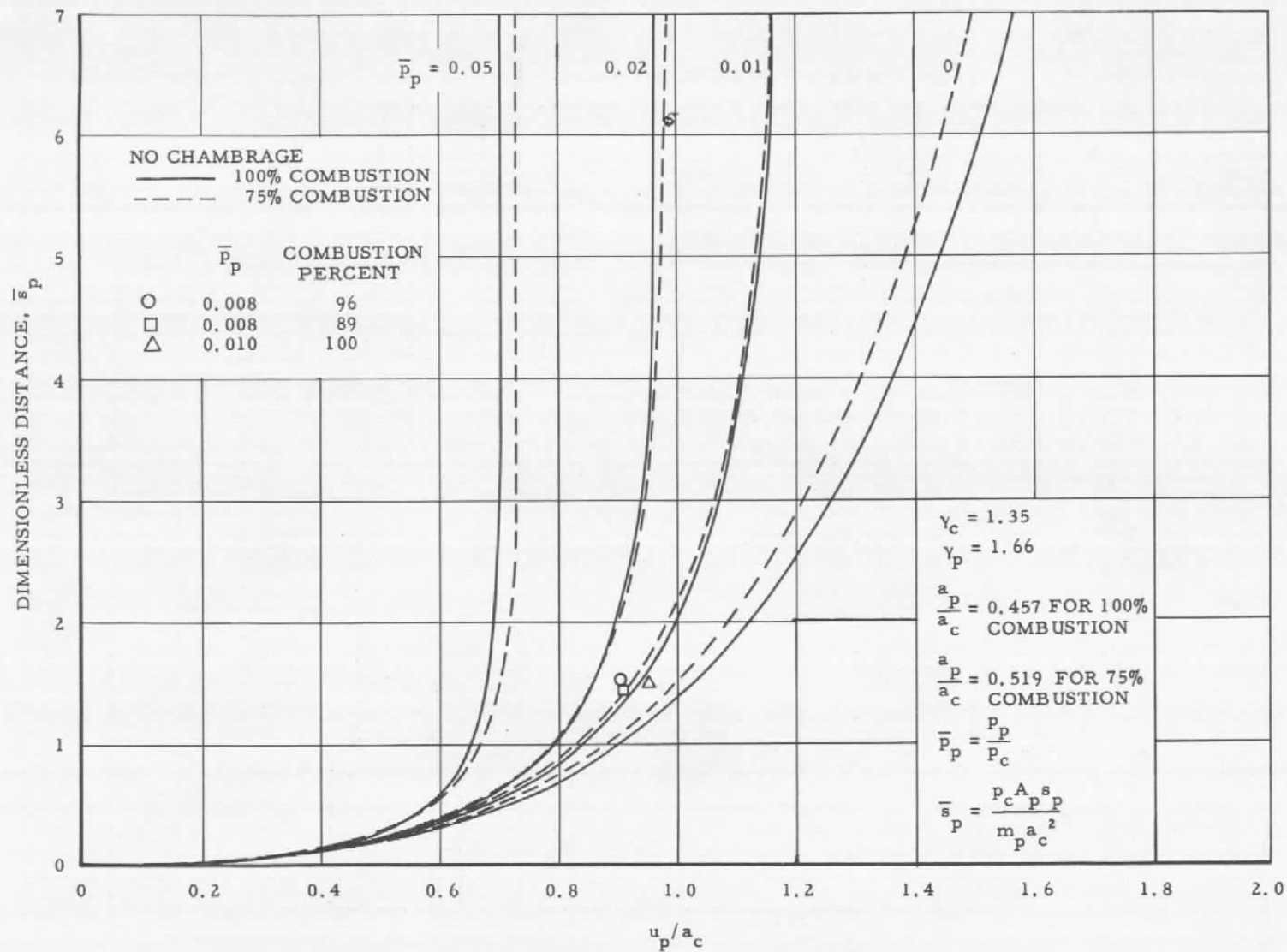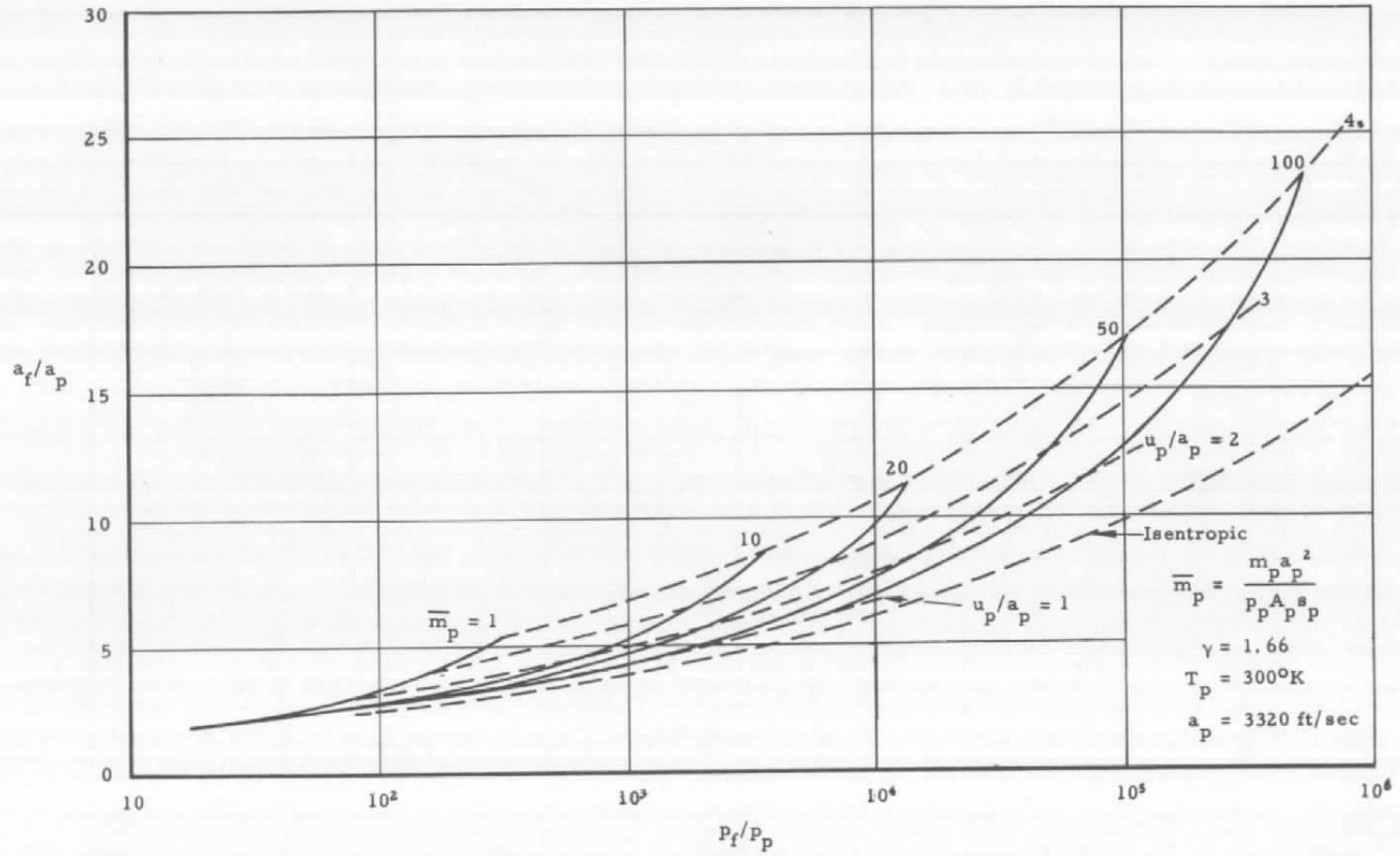
a. Final State of Helium in Pump Tube

Fig. 7 General Pump Tube Characteristics

a_f/a_p

3.4

3.2

1.8

1.6 1.4

3.0

$u_p/a_p = 1.2$

2.8

2.6

10   15

$\overline{m}_p = 5$

20

2.4

$u_p/a_p = 1.0$

$$\overline{m}_p = \frac{m_p a_p^2}{p_p A_p s_p}$$

2.2

p_p = 20 ATM
CURVE APPROX FOR
p_p = 10 to 100 ATM

$T_p = 300°K$

2.0

a_p = 4330 ft/sec

100   200   400   600 800 1000   2000   4000   6000

p_f/p_p

b.   Final State of Hydrogen in Pump Tube

Fig. 7 Concluded
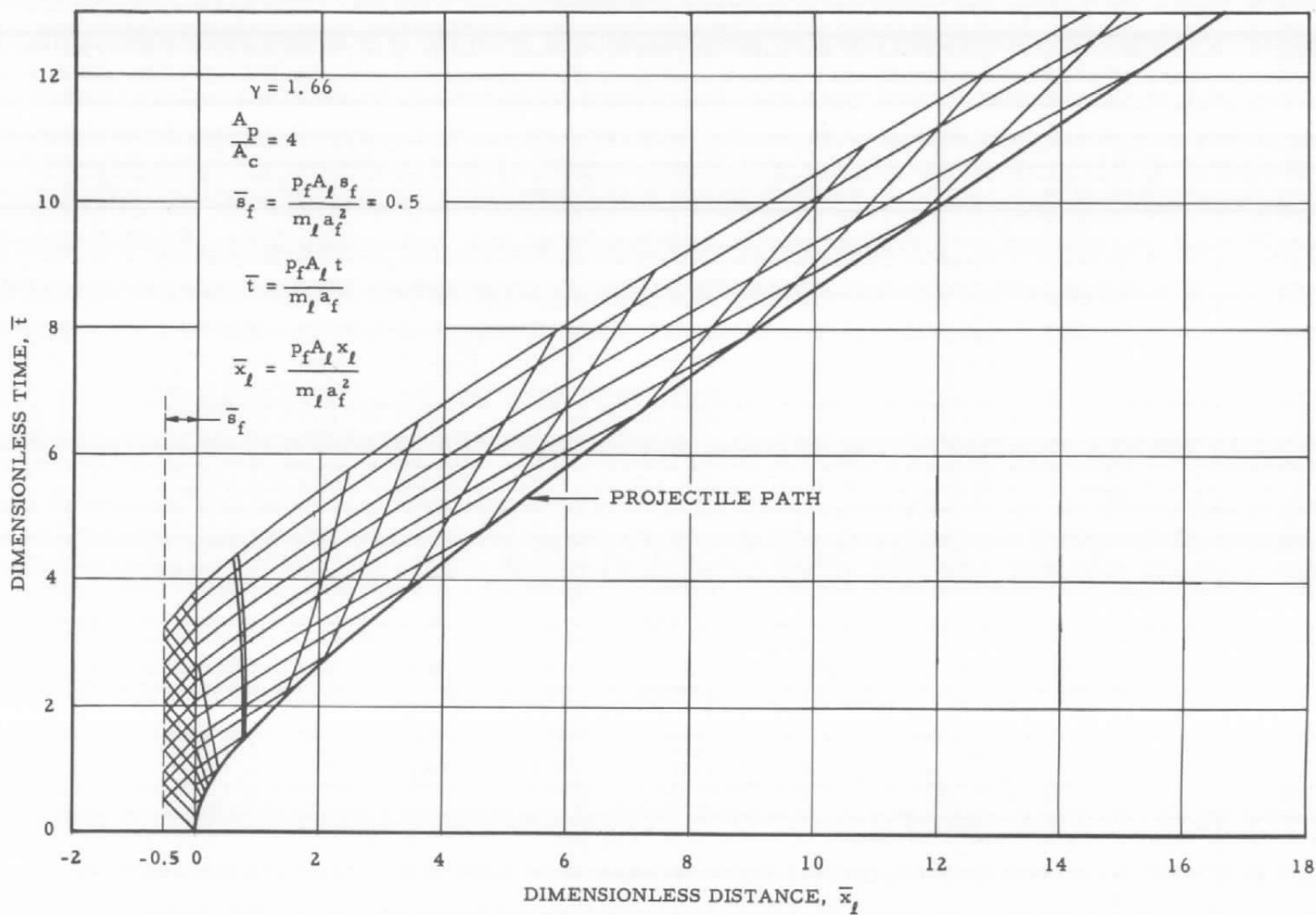
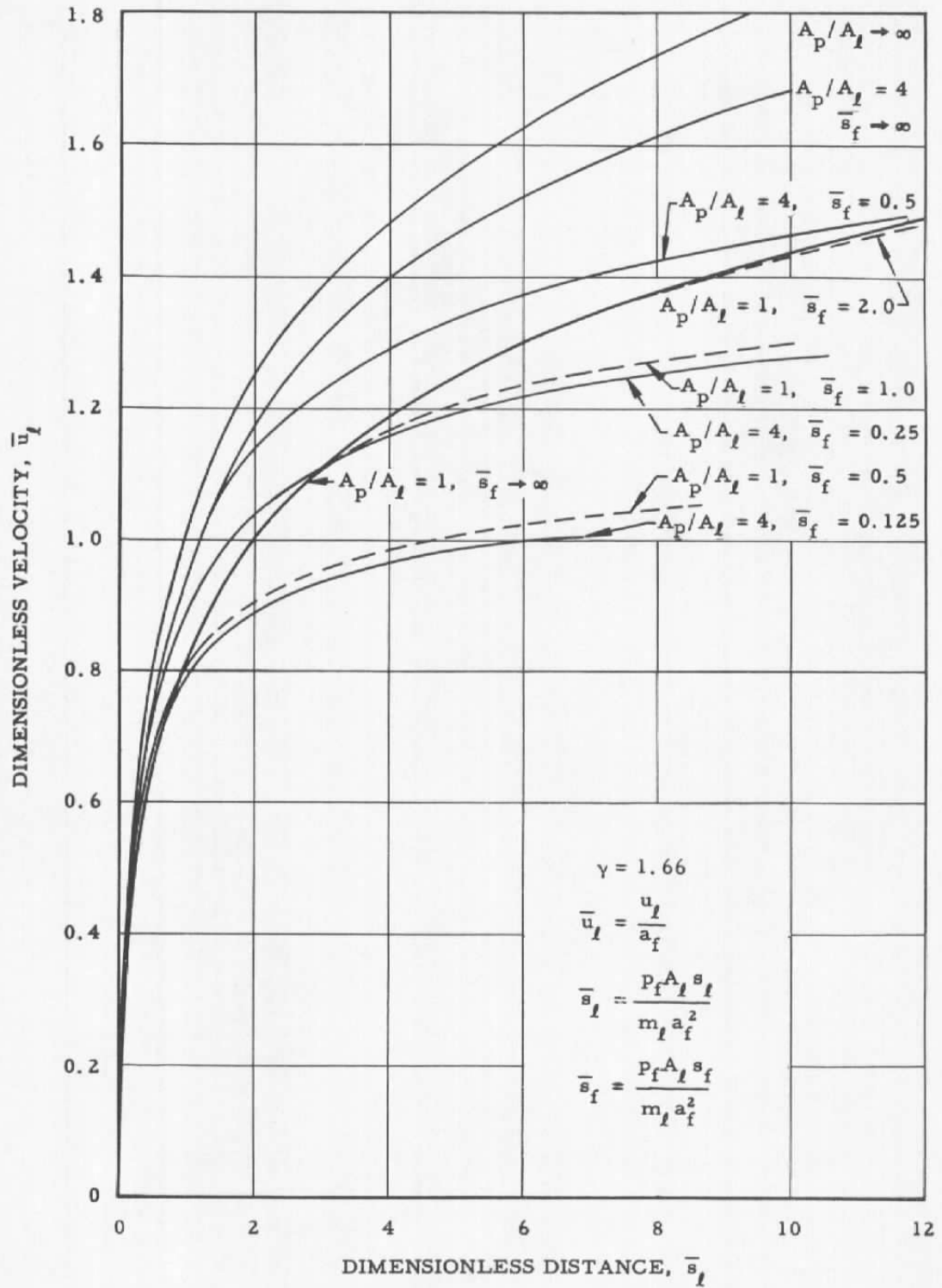Fig. 8 Typical Characteristics Network for Computation of Projectile Velocity

$$\gamma = 1.66$$

$$\frac{A_p}{A_c} = 4$$

$$\bar{s}_f = \frac{p_f A_\ell s_f}{m_\ell a_f^2} = 0.5$$

$$\bar{t} = \frac{p_f A_\ell t}{m_\ell a_f}$$

$$\bar{x}_\ell = \frac{p_f A_\ell x_\ell}{m_\ell a_f^2}$$

$\bar{s}_f$

PROJECTILE PATH

Axis labels: DIMENSIONLESS TIME, $\bar{t}$ (vertical); DIMENSIONLESS DISTANCE, $\bar{x}_\ell$ (horizontal)

Fig. 9 Effect of Chamber Geometry on Projectile Velocity
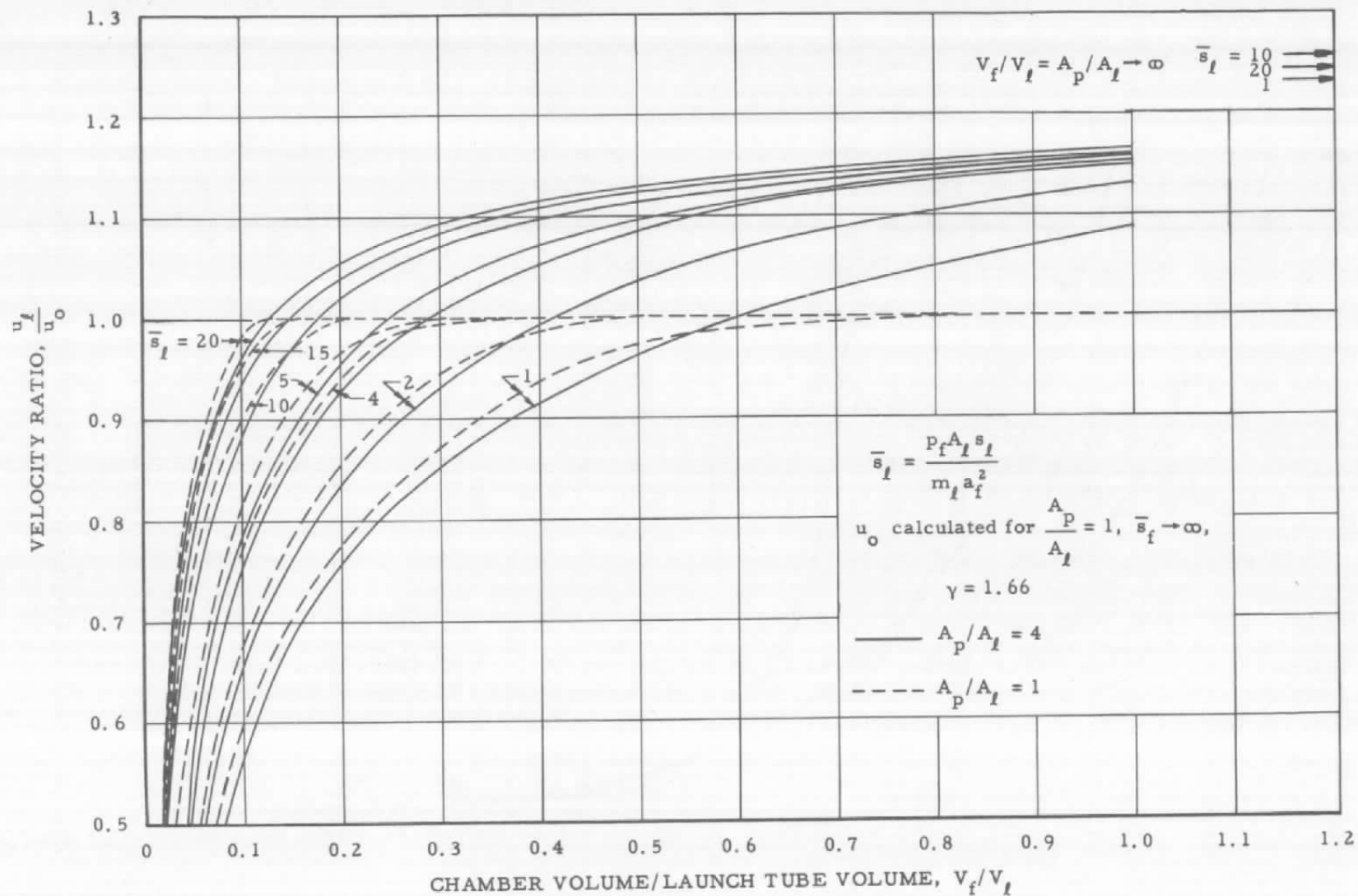
Fig. 10 Effect of Chamber/Launch Tube Volume Ratio on Launch Velocity

COMBUSTION CHAMBER
2.75 ID, 8 OD

PUMP TUBE
1.58 ID, 5 OD

HIGH PRESSURE SECTION
1.58 ID, 6 OD

LAUNCH TUBE
0.5 ID, 2.5 OD

|← 44 →|← 126 →|← 115 →|

IGNITION WIRE

PISTON

DIAPHRAGM

MIXER FOR GAS CHARGING

PROJECTILE

BREECH PLUG

ALL DIMENSIONS IN INCHES
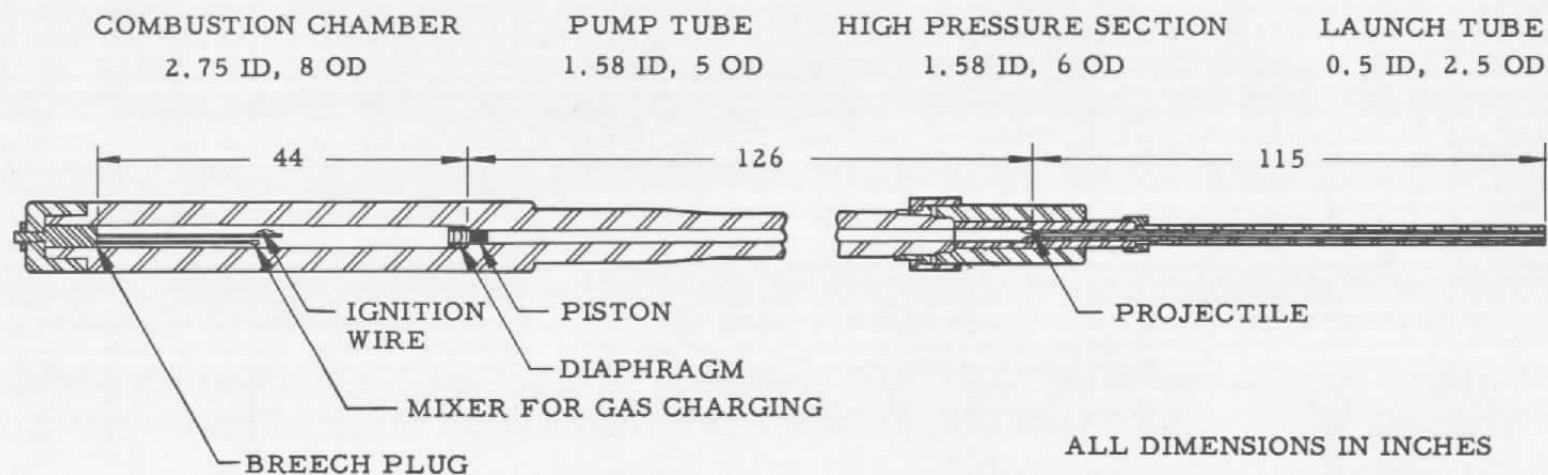
Fig. 11 One-Half Inch Diameter, Two-Stage Launcher
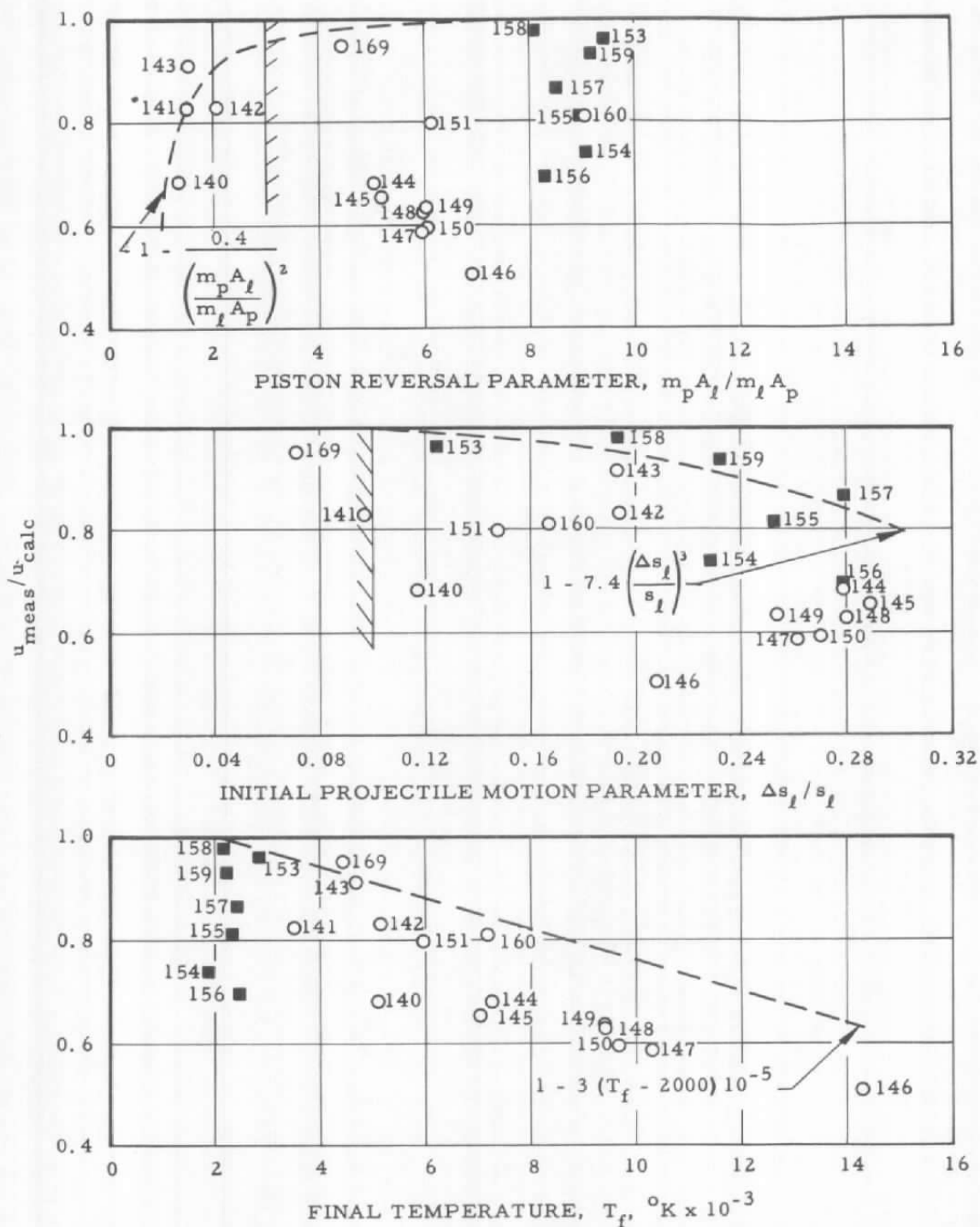
Fig. 12 Determination of Corrections

CORRELATION FORMULA:

$$\frac{u}{u_{calc}} = 1 - \frac{0.4}{\left(\frac{m_p A_l}{m_l A_p}\right)^2} - 7.4 \left(\frac{\Delta s_l}{s_l}\right)^3 - 3 \, (T_f(^{o}K) - 2000) \, 10^{-5}$$
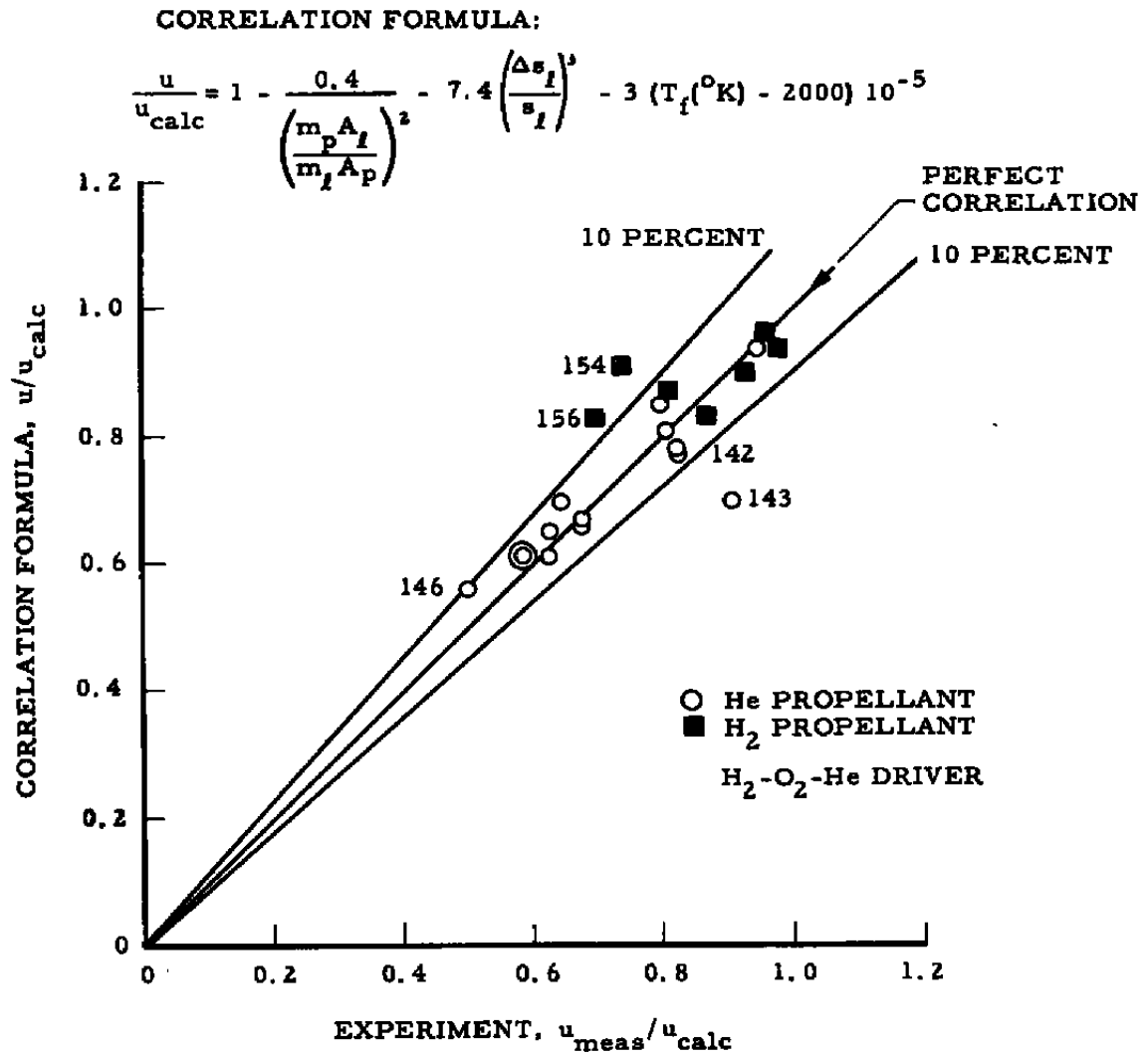
Fig. 13 Correlation of Experimental Results
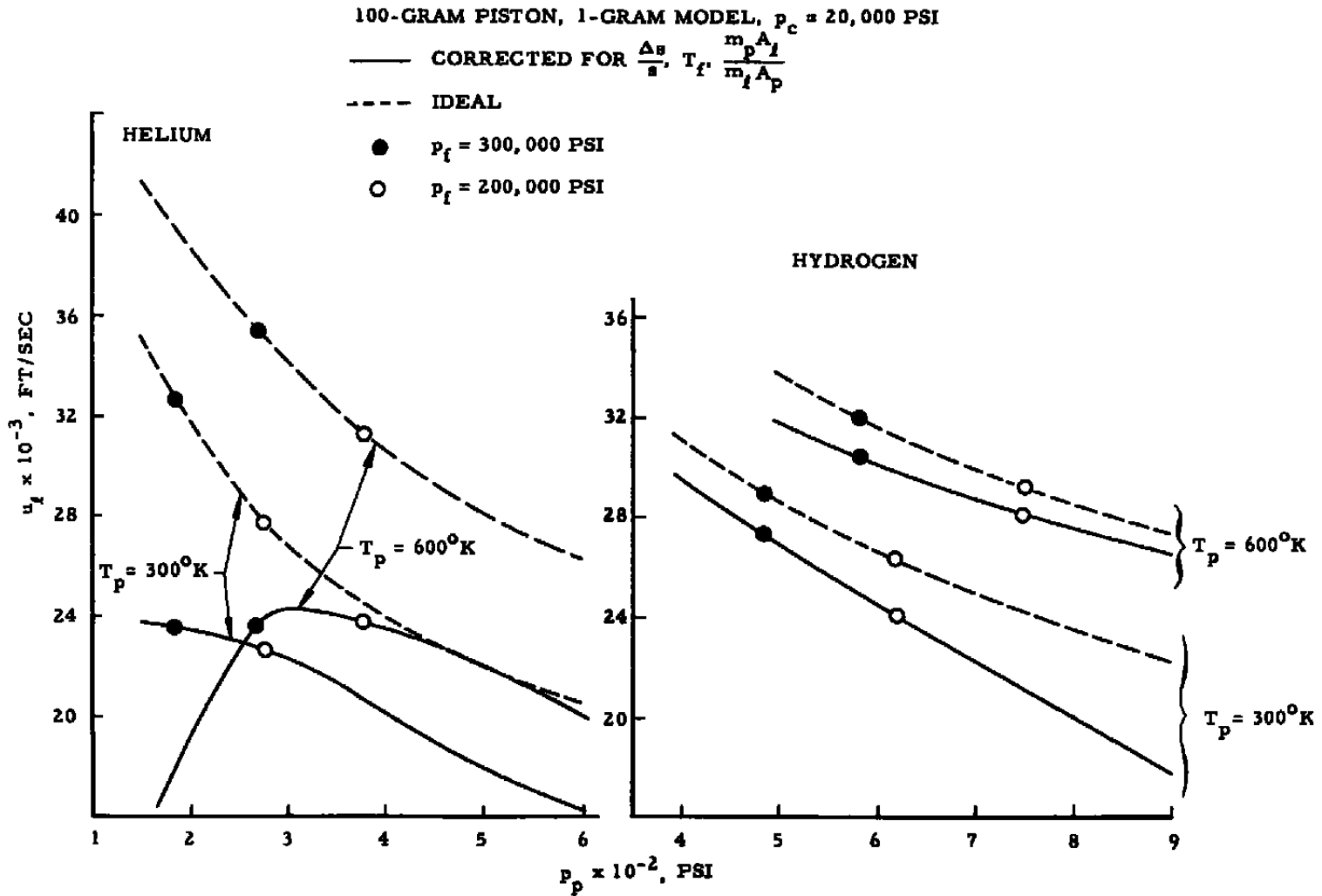
Fig. 14 Estimated Performance of 0.5-Inch Two-Stage Launcher
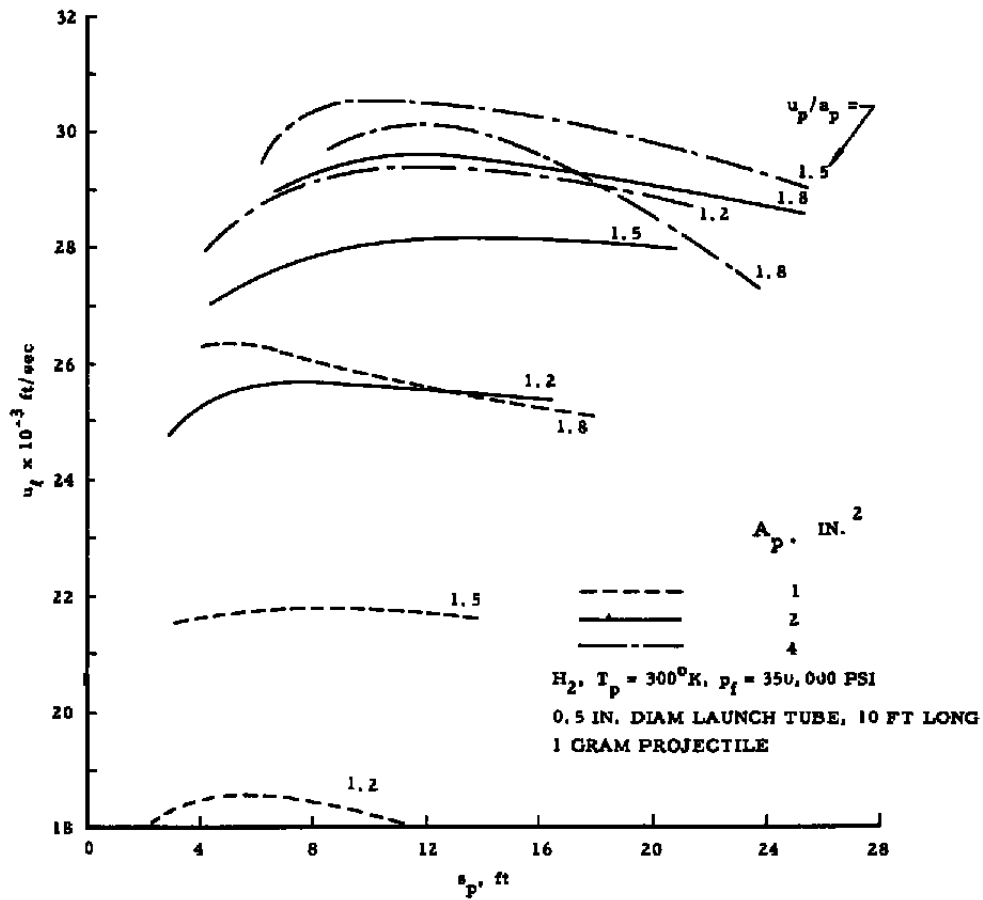
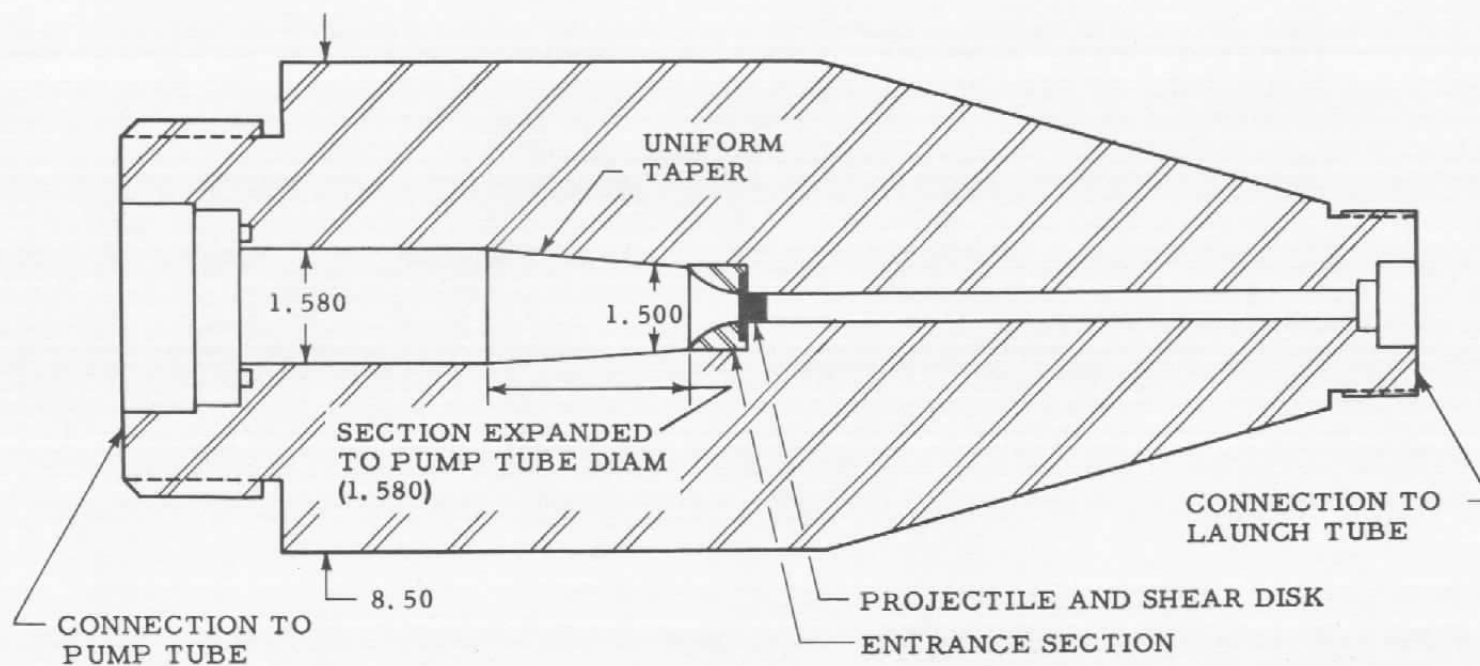Fig. 15 Effect of Pump Tube Dimensions on Launch Velocity

OVERSTRAIN CONDITION IS DEFINED
AS THE POINT WHEN PLASTIC FLOW
HAS PROGRESSED TO THE OUTER
RADIUS.
σ_y = YIELD STRENGTH IN TENSION

$E = 30 \times 10^6$ psi

$\sigma_y = 200,000$ psi

180,000

160,000

INTERNAL PRESSURE AT OVERSTRAIN CONDITIONS, p_{os}/σ_y

INTERNAL GROWTH AT OVERSTRAIN CONDITIONS, ϵ_{os}/a

RADIUS RATIO, b/a

Fig. 16 Auto-Frettaging Curves

UNIFORM
TAPER

1.580

1.500

SECTION EXPANDED
TO PUMP TUBE DIAM
(1.580)

8.50

CONNECTION TO
PUMP TUBE

CONNECTION TO
LAUNCH TUBE

PROJECTILE AND SHEAR DISK

ENTRANCE SECTION

Fig. 17 High Pressure Section before Auto-Frettaging
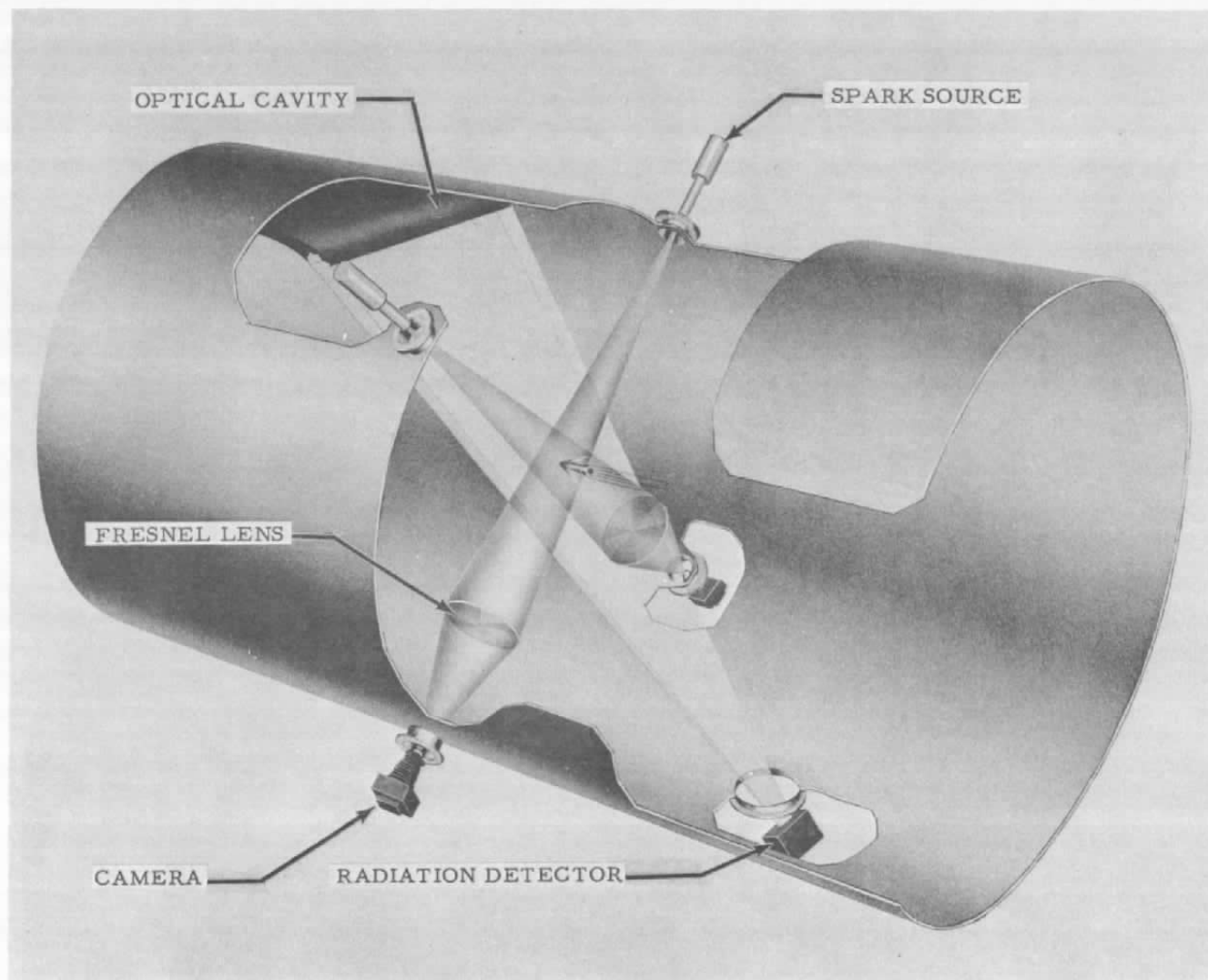
Fig. 18 Dual, Fresnel Lens, Shadowgraph Installation

VELOCITY: 5300 fps
RANGE TANK PRESSURE: 38 mm
PROJECTILE LENGTH: 67 mm
PROJECTILE DIAMETER: 40 mm

Fig. 19a Fresnel Lens Shadowgram

VELOCITY: 11,400 fps
RANGE TANK PRESSURE: 20 mm
PROJECTILE LENGTH: 40 mm
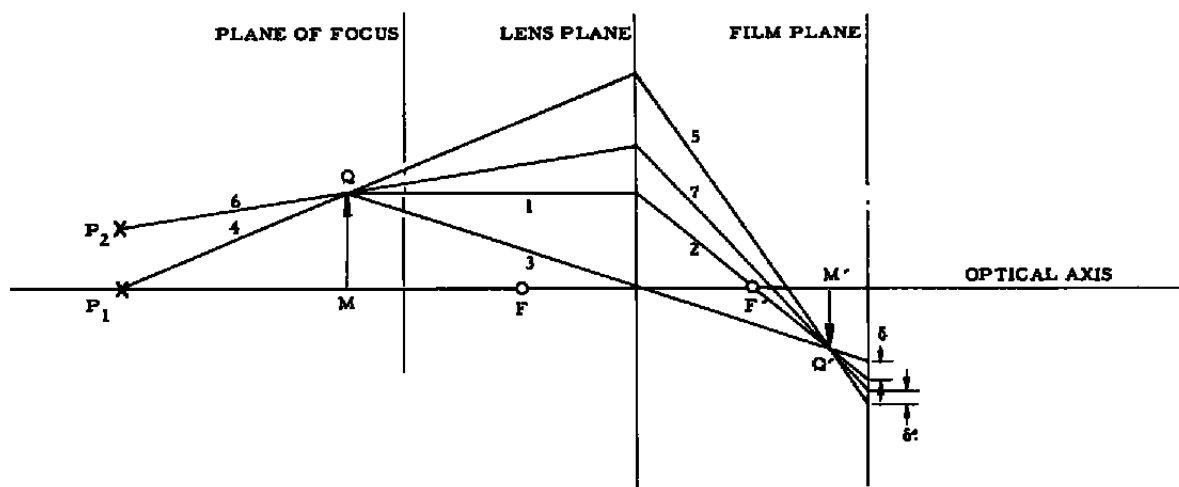PROJECTILE DIAMETER: 40 mm

FLIGHT

b
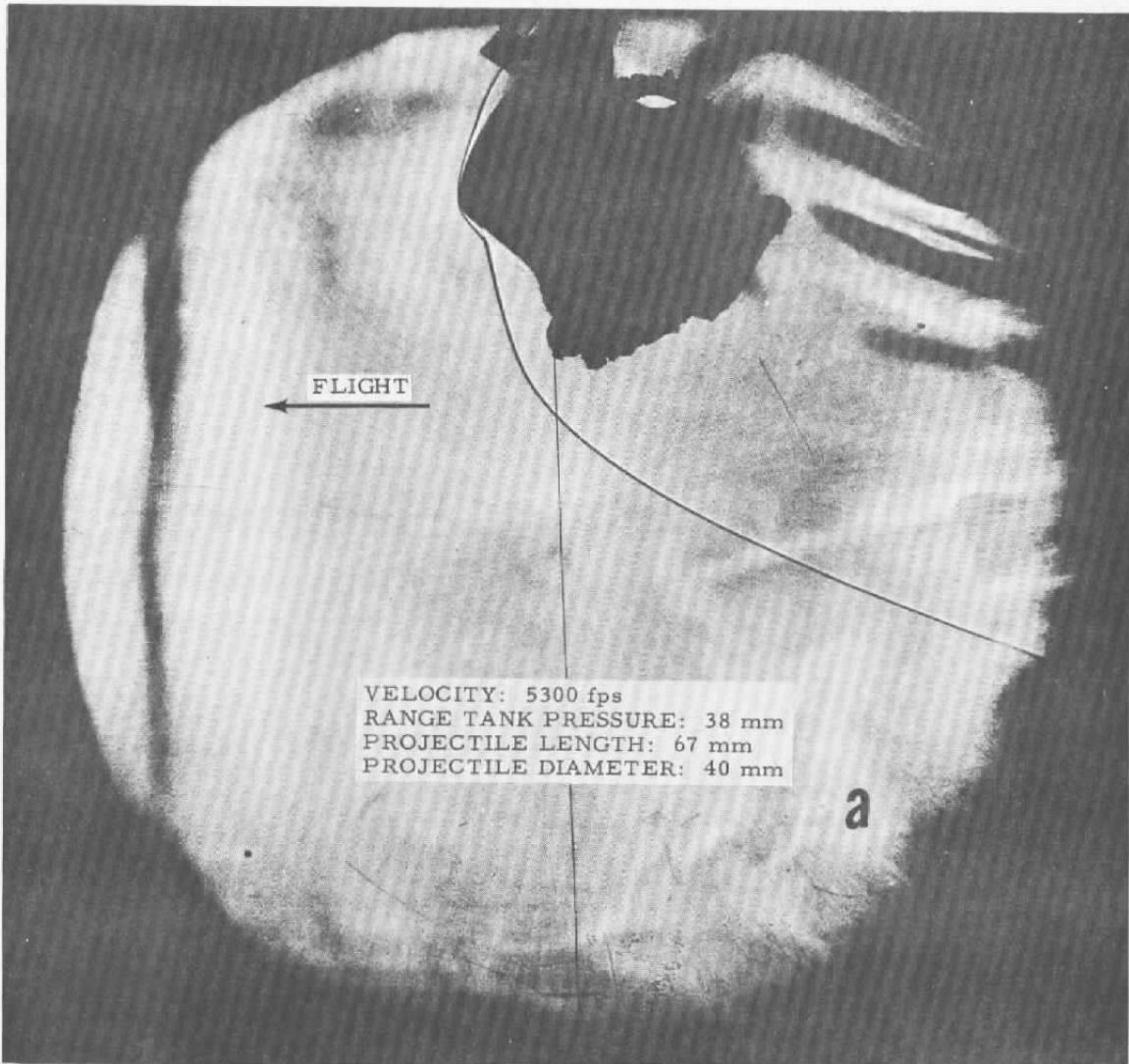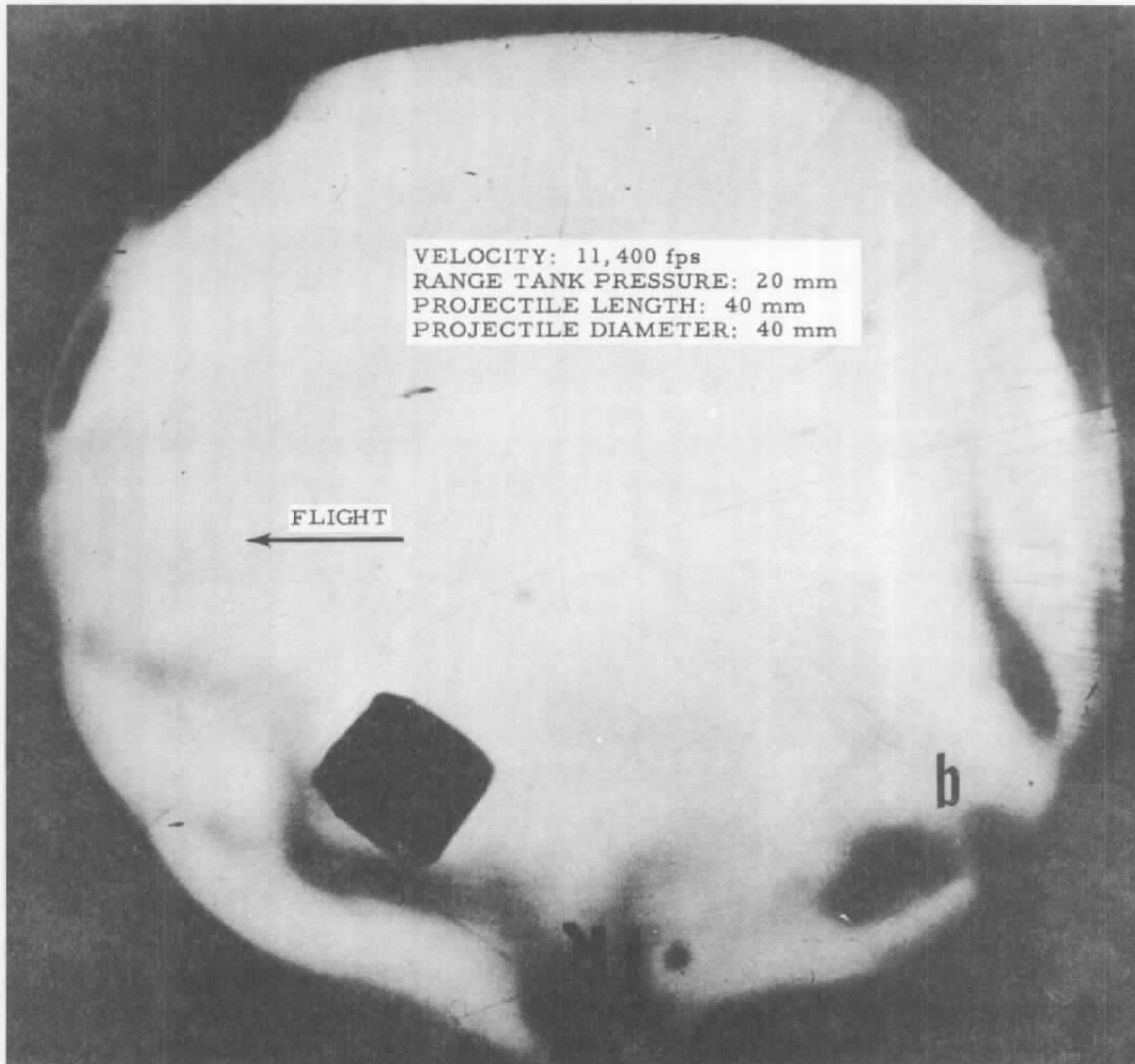
Fig. 19b Fresnel Lens Shadowgram
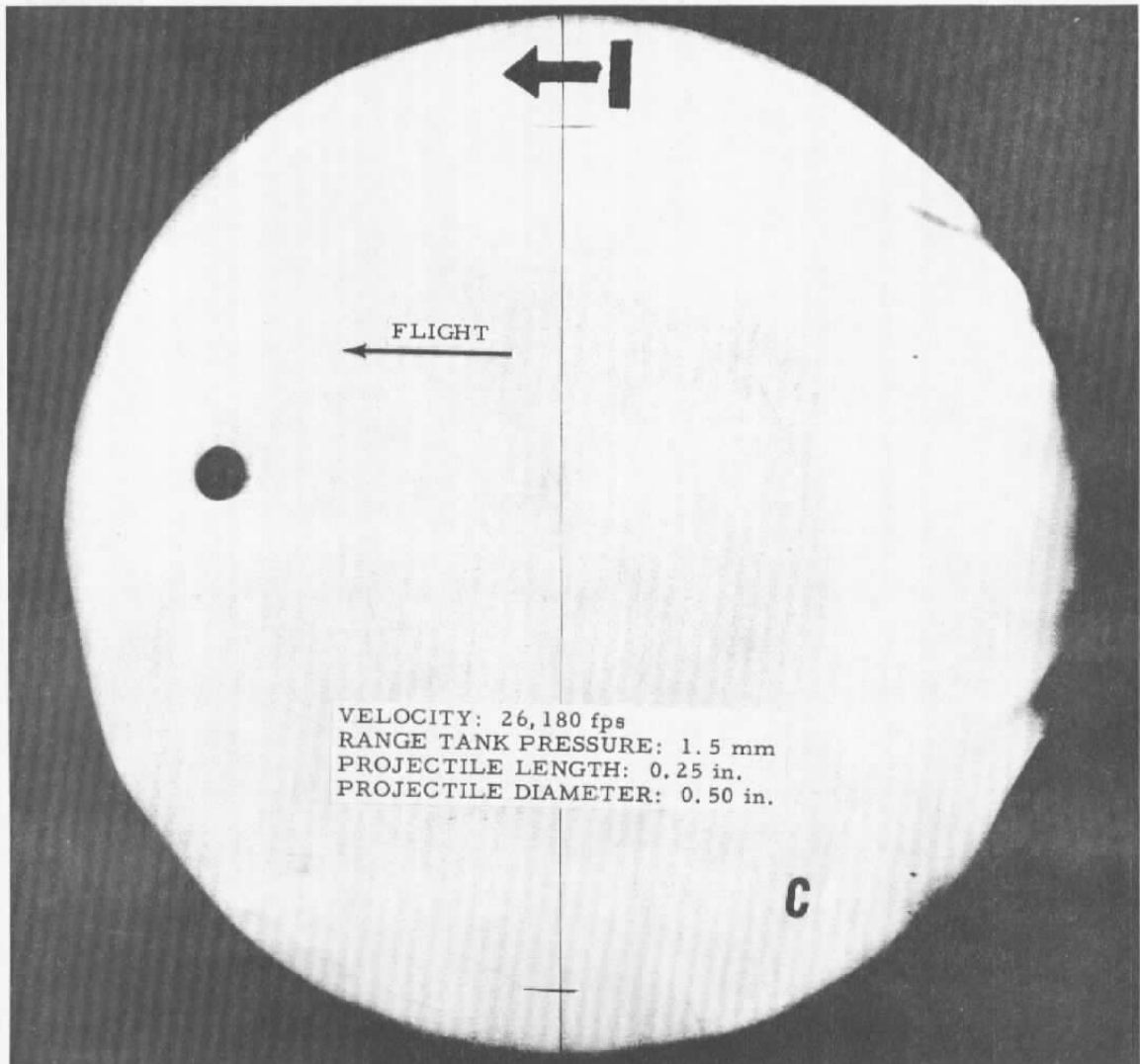
Fig. 19c Fresnel Lens Shadowgram
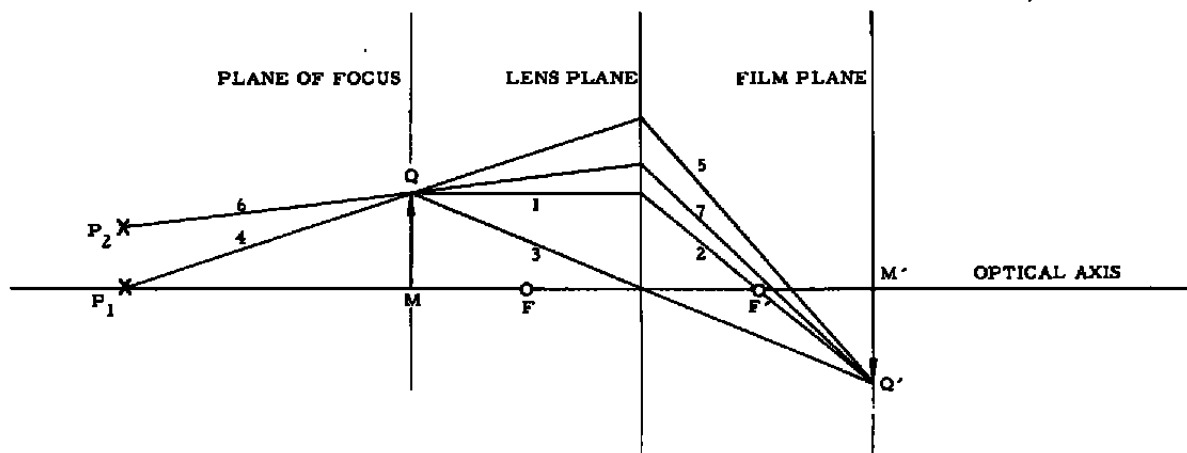
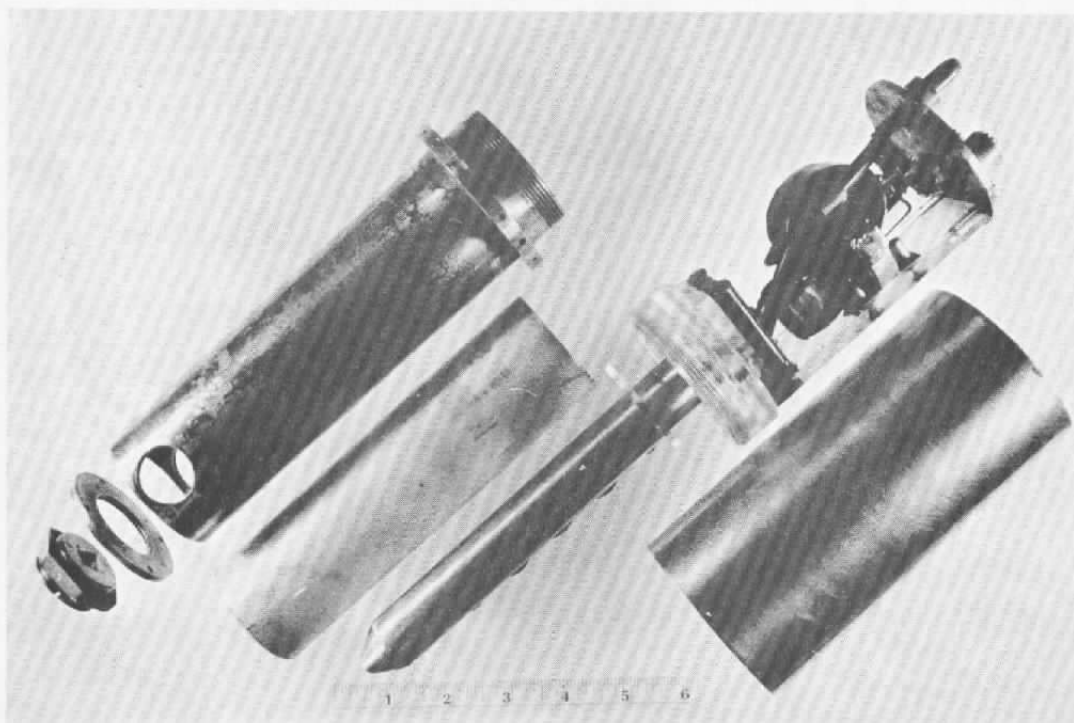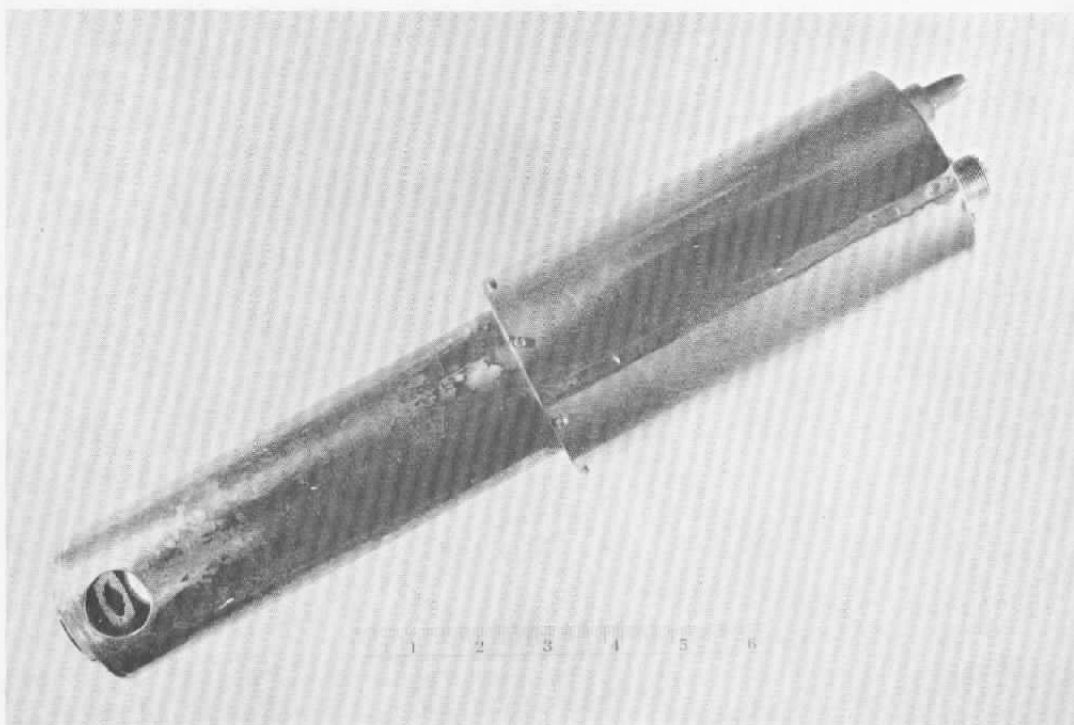a. Object in Plane of Focus

b. Object Not in Plane of Focus

Fig. 20 Graphic Analysis of Fresnel Lens Shadowgraph

a. Disassembled

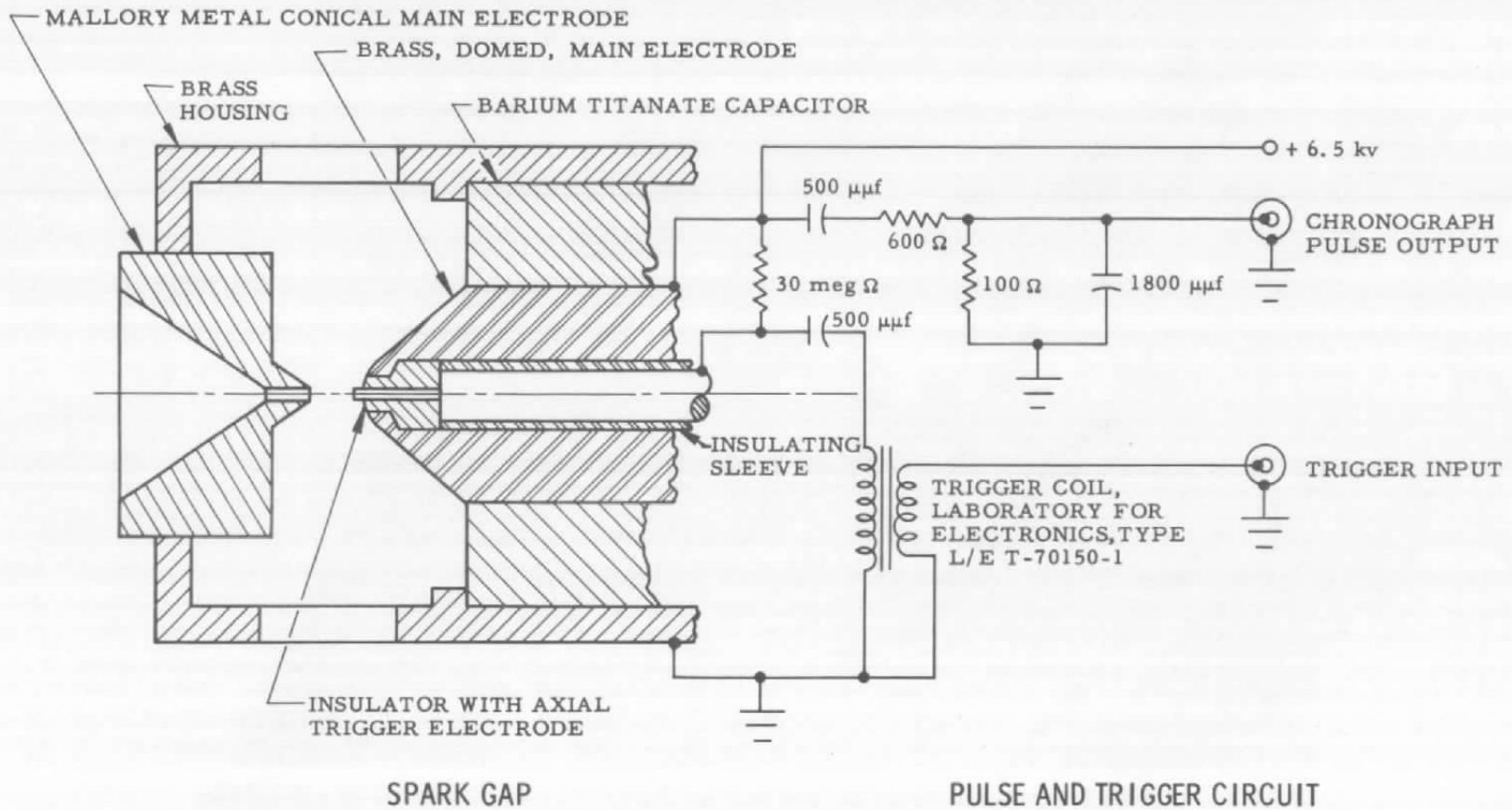b. Assembled
Fig. 21 Shadowgraph Spark Source

Fig. 22 Shadowgraph Spark Source Structure and Circuit

FLIGHT

VELOCITY: 11,980 fps
RANGE TANK PRESSURE: 28 mm
PROJECTILE LENGTH: 40 mm
PROJECTILE DIAMETER: 40 mm

Fig. 23 Fresnel Lens Shadowgram without Blue Filter

+ 6.5 v

- 67.5 v

10 kΩ 8.2 kΩ 0.05 µf 82 kΩ 33 kΩ 22 kΩ 27 kΩ 24 kΩ 150 kΩ 50 kΩ 1 megΩ 39 kΩ

Q1 0.05 µf Q2 0.05 µf 0.05 µf Q3 0.05 µf Q4 0.05 µf Q5 0.05 µf Q6 0.05 µf OUTPUT

910 kΩ 10 kΩ 30 kΩ 20 kΩ 20 kΩ 16 kΩ 5 µf 27 kΩ 27 kΩ 5 µf 13 kΩ 20 kΩ 5 µf 39 kΩ 68 kΩ 5 µf

OUTPUT

Q1 = 2N469A, PHOTO-TRANSISTOR
Q2-5 = 2N167
Q6 = 2N1226
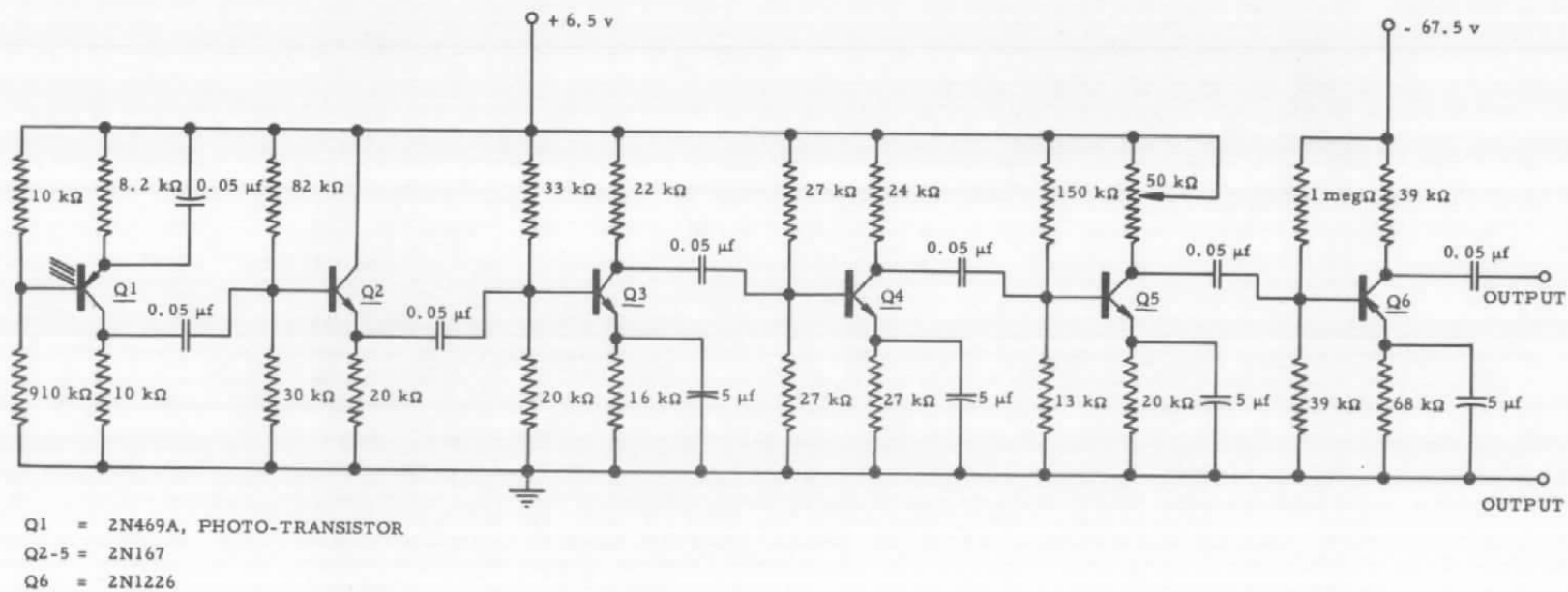
Fig. 24 Transistorized Radiation Detector Circuit
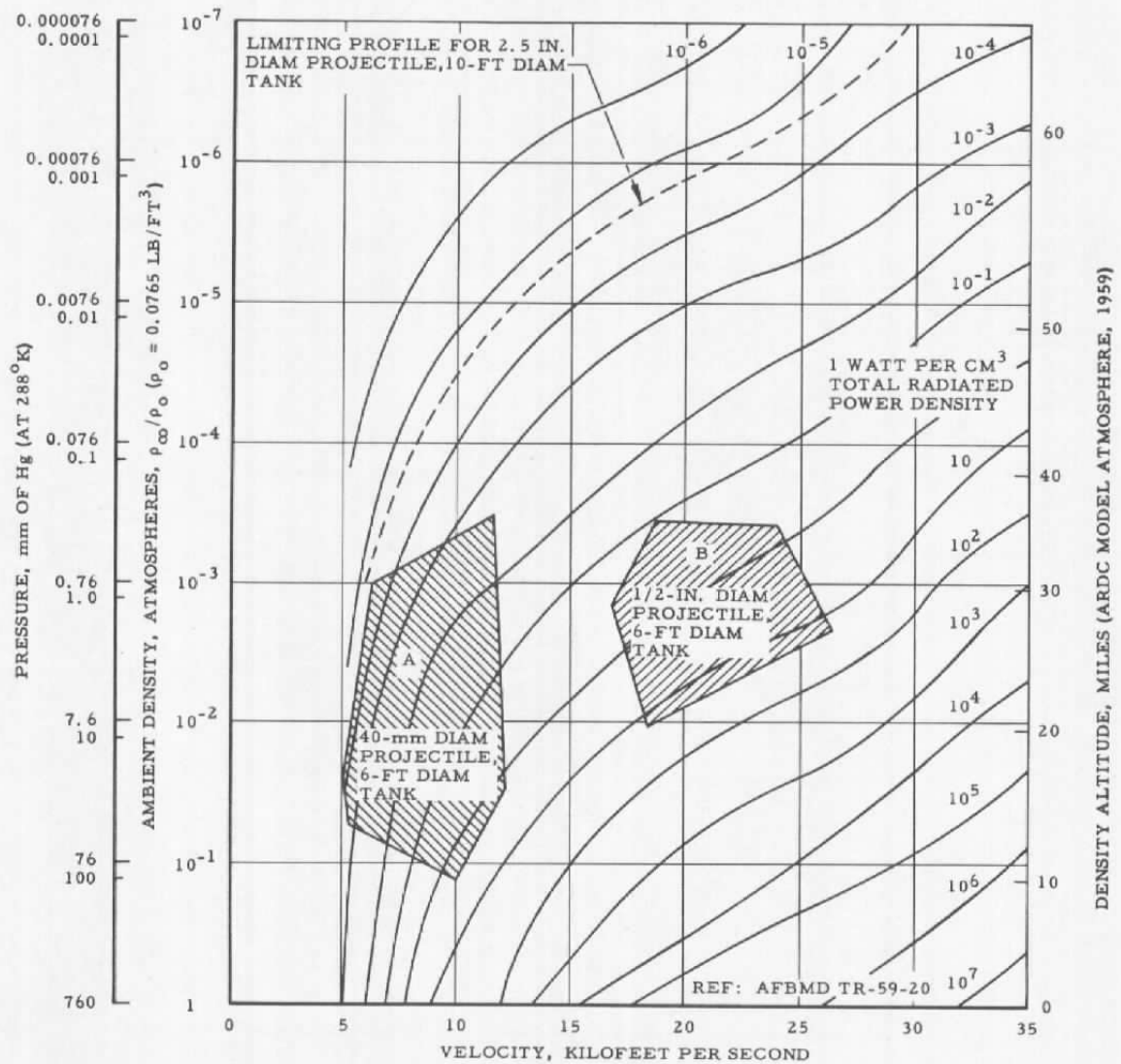
Fig. 25 Radiation Detector Performance

AEDC-TR-61-9

ANTENNA-OSCILLATOR
COIL**

TRANSDUCER

100 μμf

24 μμf

10 k

24 μμf

*

5.2 v

2N850
(TI451)

5 μμf

15 k

1 k
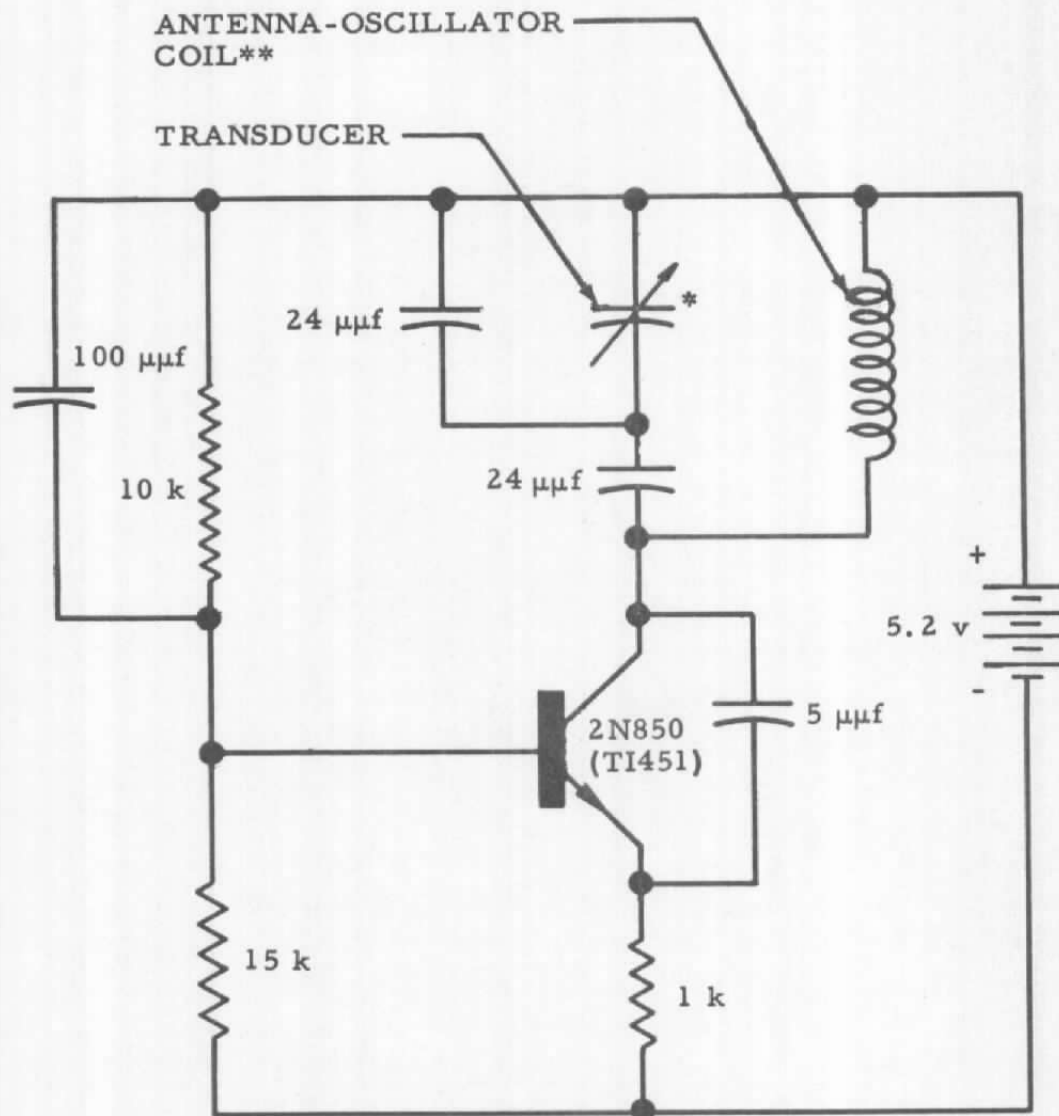
* QUIESCENT CAPACITANCE: 8 μμf
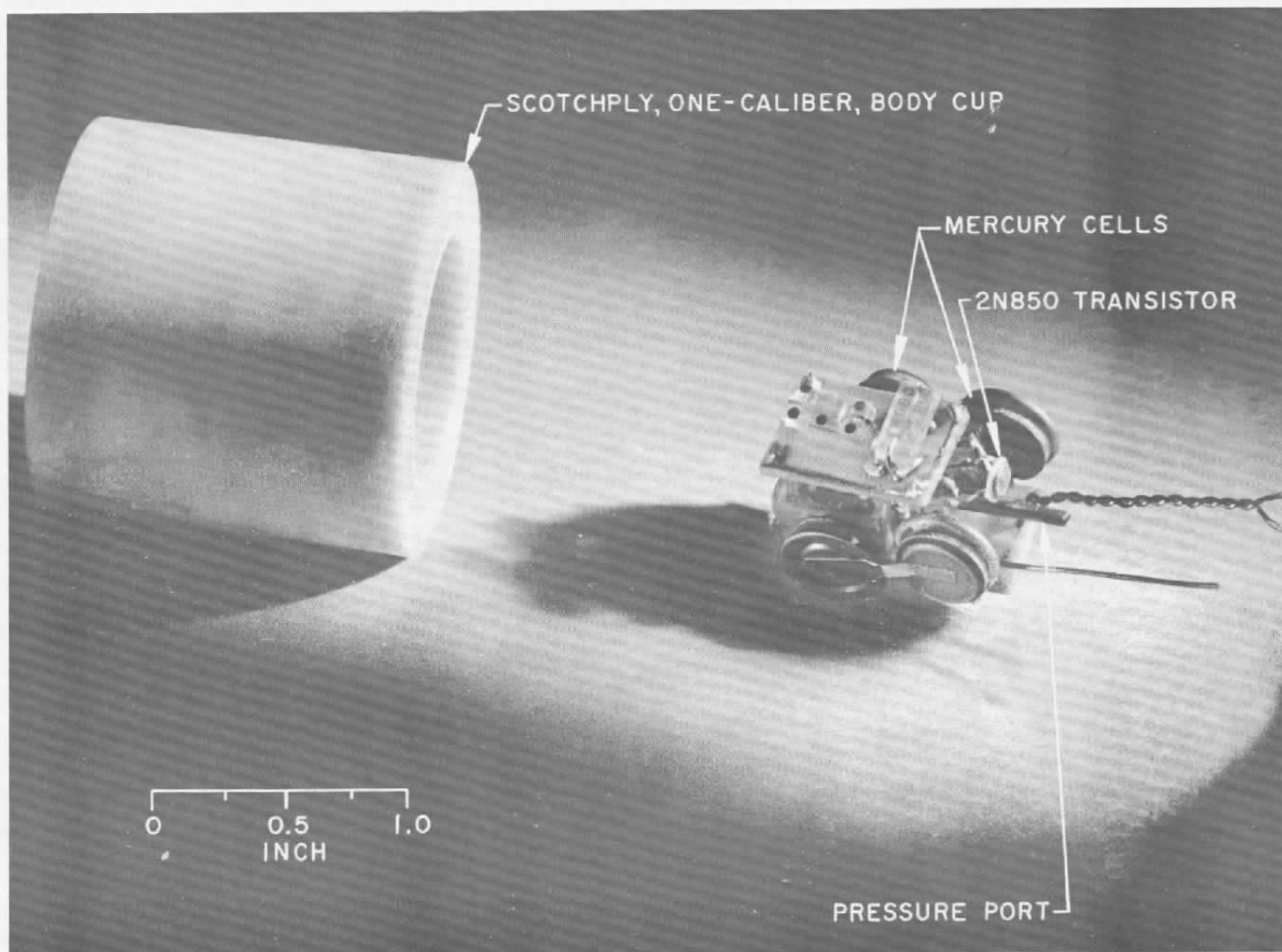** FOUR TURNS, 24 AWG WIRE,
0.16-IN. ID

Fig. 26 Pressure Telemeter Circuit
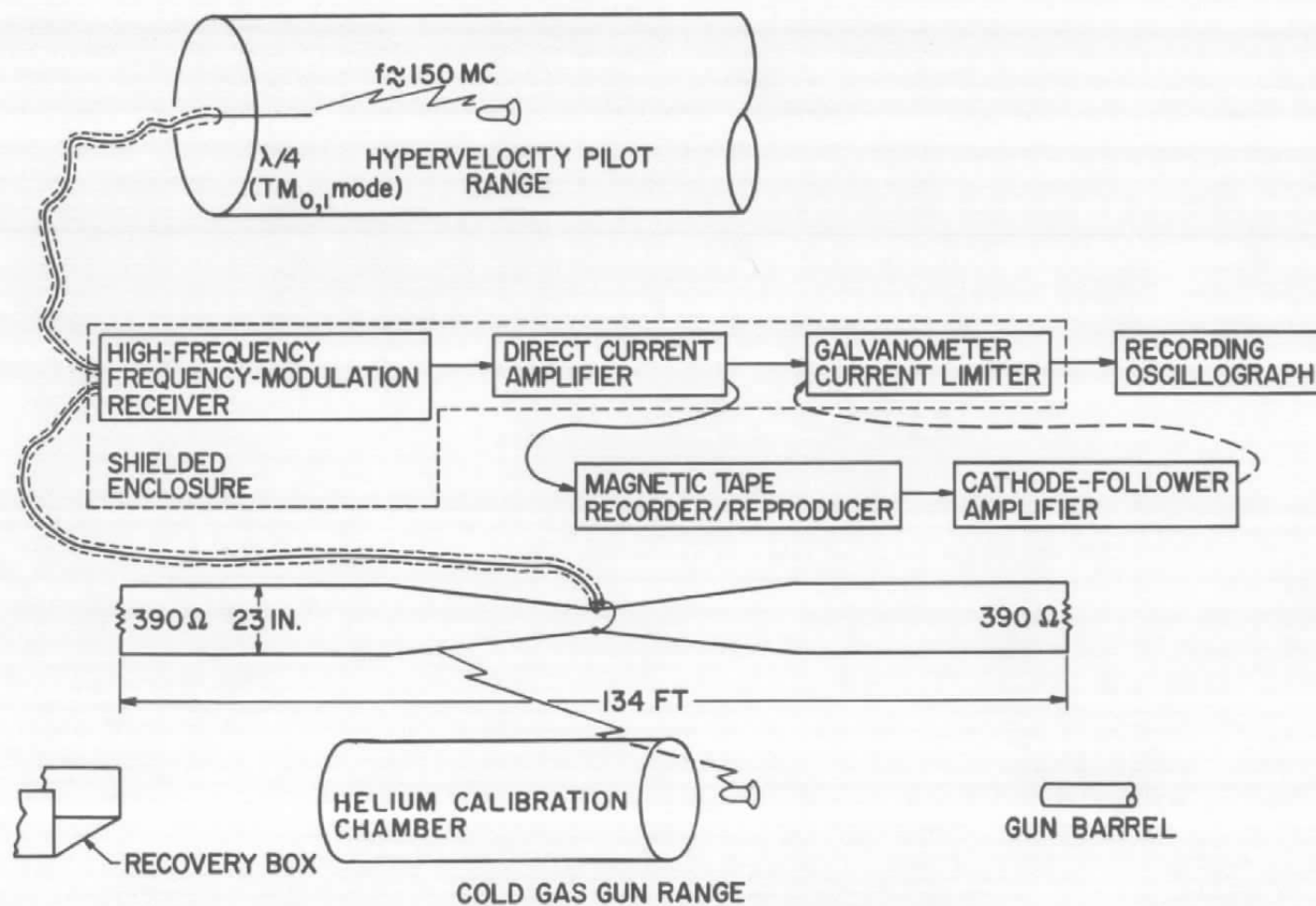
Fig. 27 Pressure Telemeter and Body Shell

Fig. 28 Telemetry Data Acquisition System
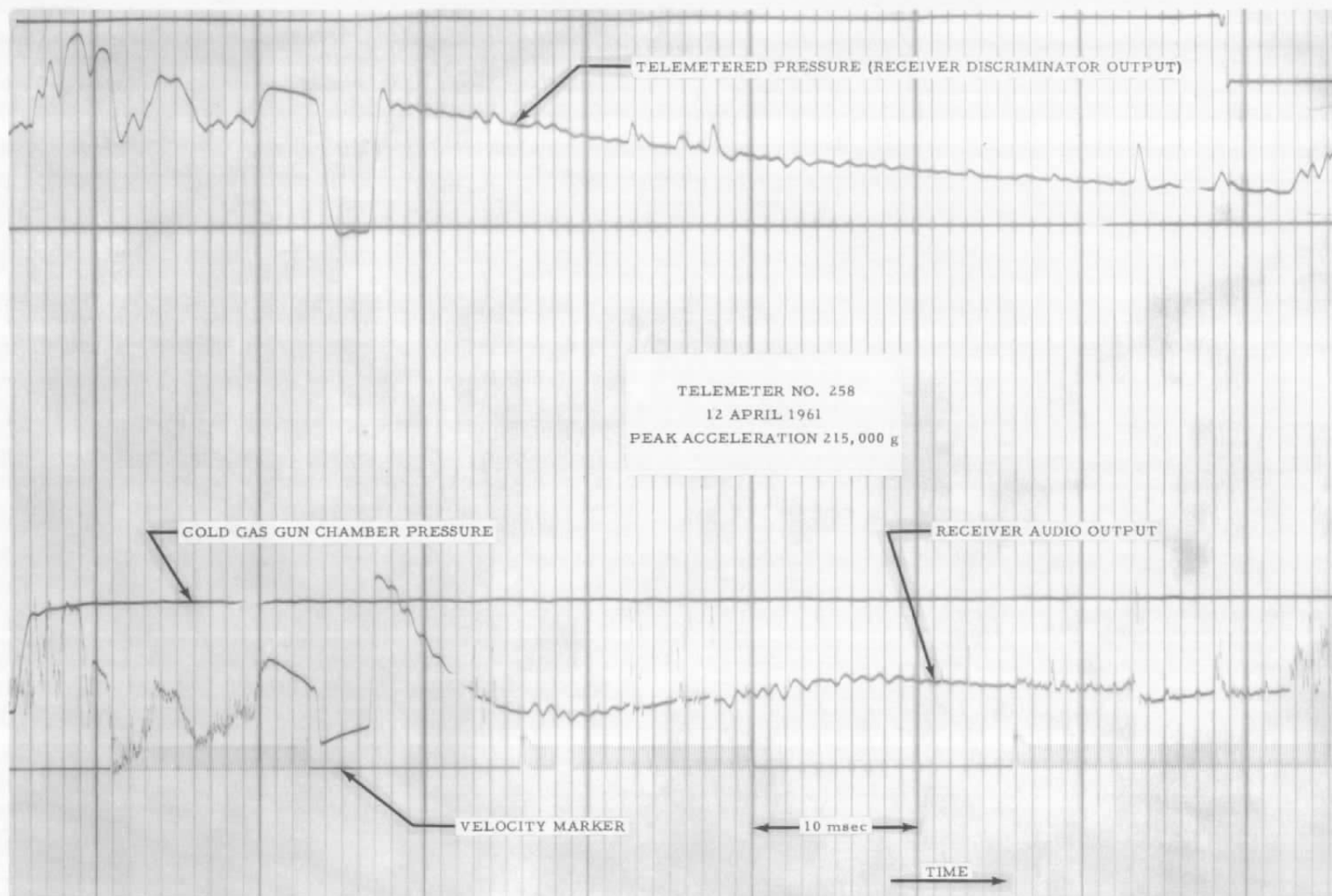
Fig. 29 Helium Calibration Chamber

TELEMETERED PRESSURE (RECEIVER DISCRIMINATOR OUTPUT)

TELEMETER NO. 258
12 APRIL 1961
PEAK ACCELERATION 215,000 g

COLD GAS GUN CHAMBER PRESSURE

RECEIVER AUDIO OUTPUT

VELOCITY MARKER

←— 10 msec —→

TIME →

Fig. 30 Pressure Telemeter Oscillogram
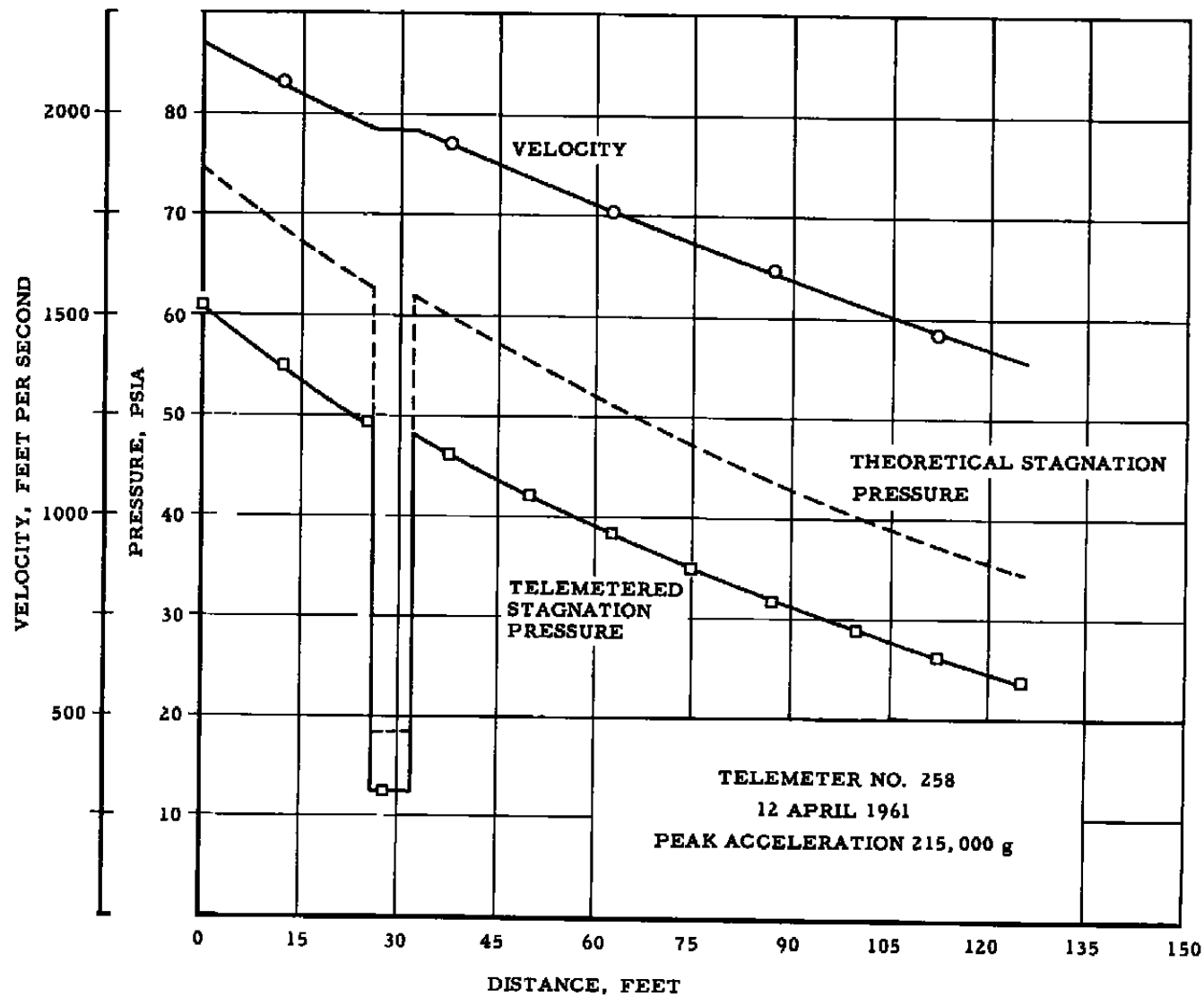
Fig. 31 Comparison of Theoretical with Telemetered Data

OUTPUT TO
MAGNETIC TAPE
RECORDING SYSTEM

CRYSTAL DETECTOR

NON-REFLECTING DUMMY LOAD

ADAPTOR: WAVEGUIDE TO
COAXIAL CABLE

POWER
SUPPLY

X-BAND DIRECTIONAL COUPLER WAVEGUIDE

VARIAN X-13
KLYSTRON
(X-BAND)

CHAMBER

BARREL

A

40 mm TELEMETER LAUNCHER

(COLD GAS GUN)

NYLON INSERT

COAXIAL CONNECTOR

3/8"

0.42"

16-GAGE WIRE
LOOP

LOOP PROBE

DETAIL A

Fig. 32 Microwave Reflectometer

72

CRYSTAL DETECTOR OUTPUT VOLTAGE, e_o

2. 06 in.

COMMENCEMENT OF PROJECTILE MOTION
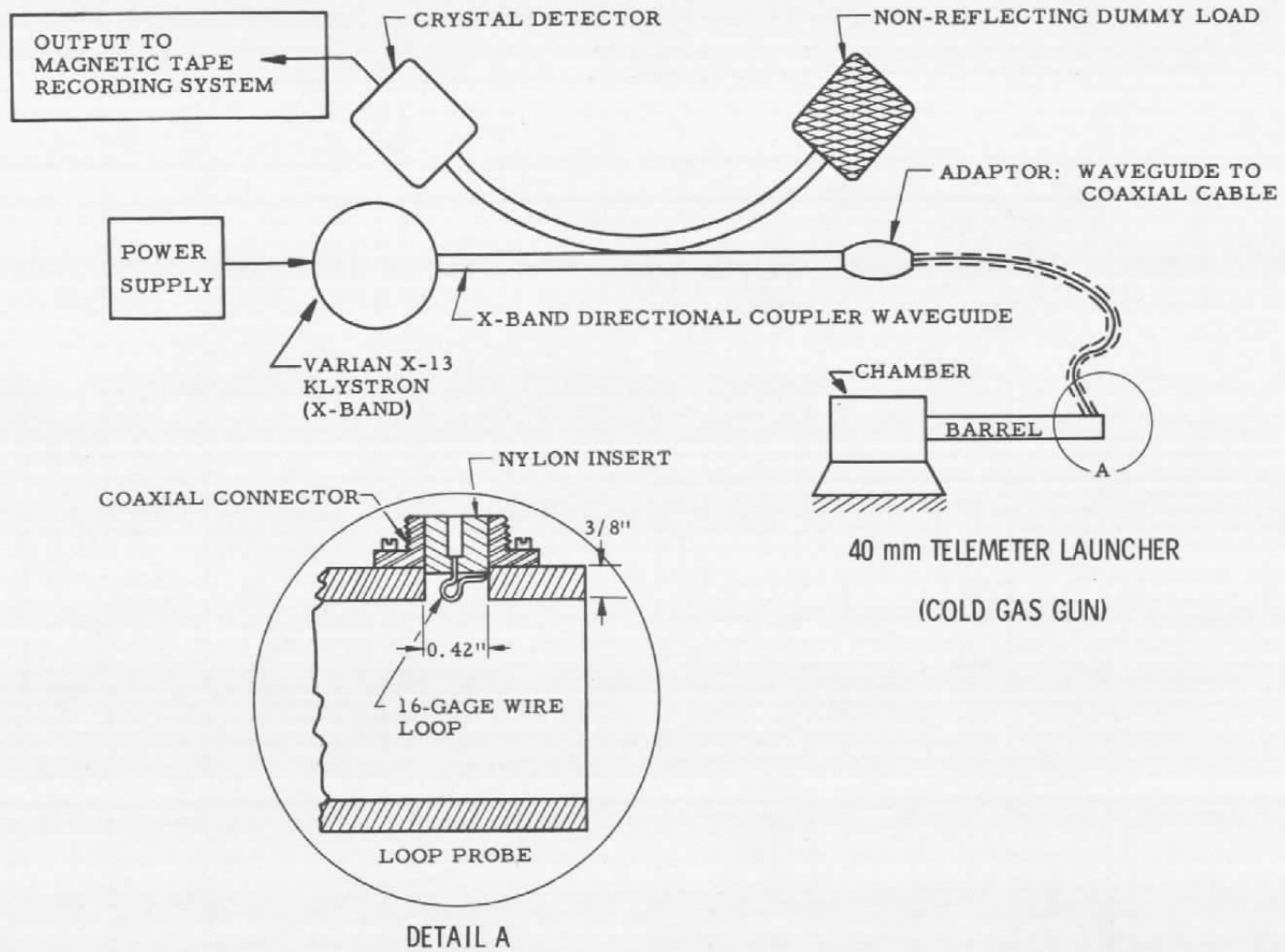
EXIT OF PROJECTILE FROM BARREL
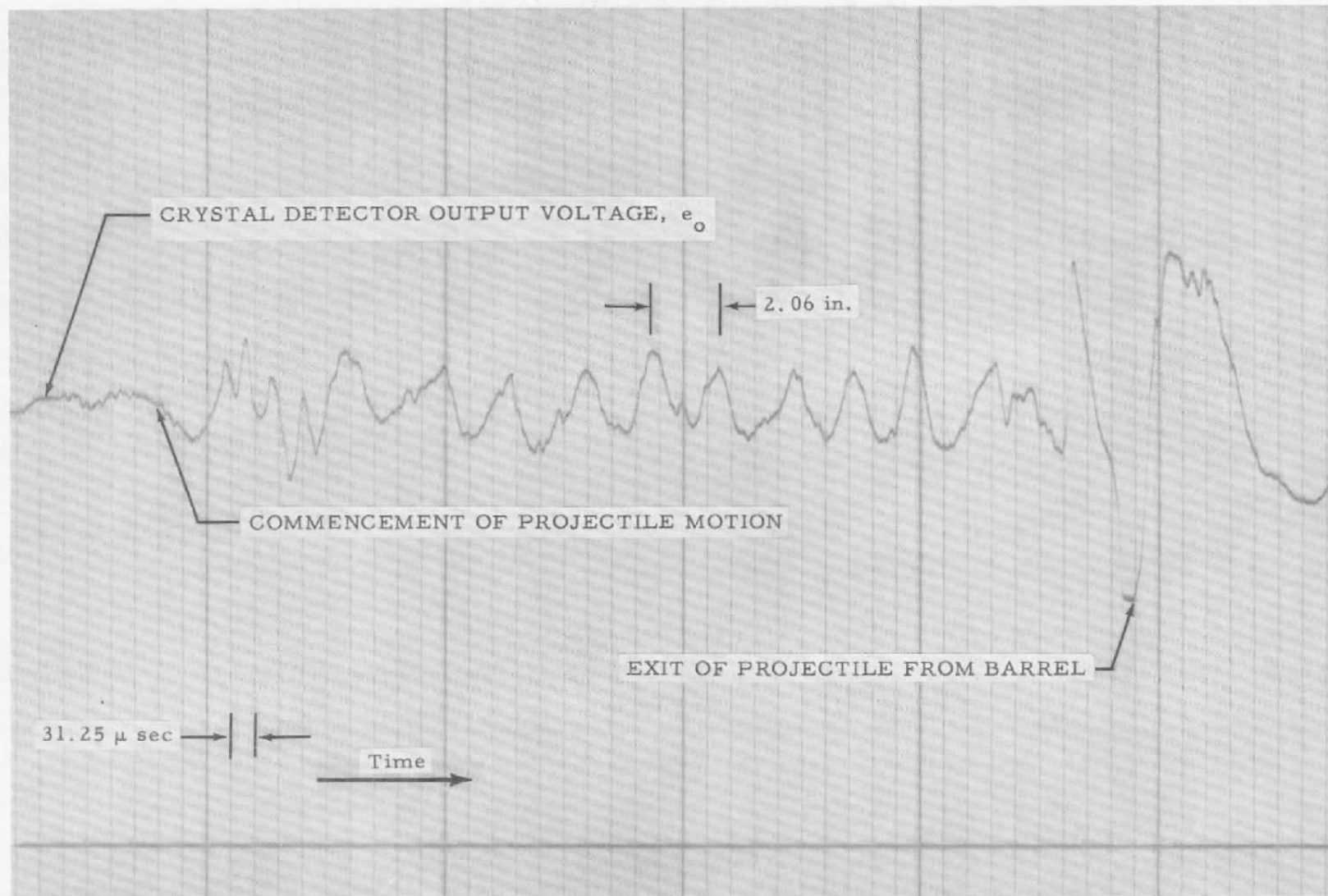
31.25 μ sec

Time

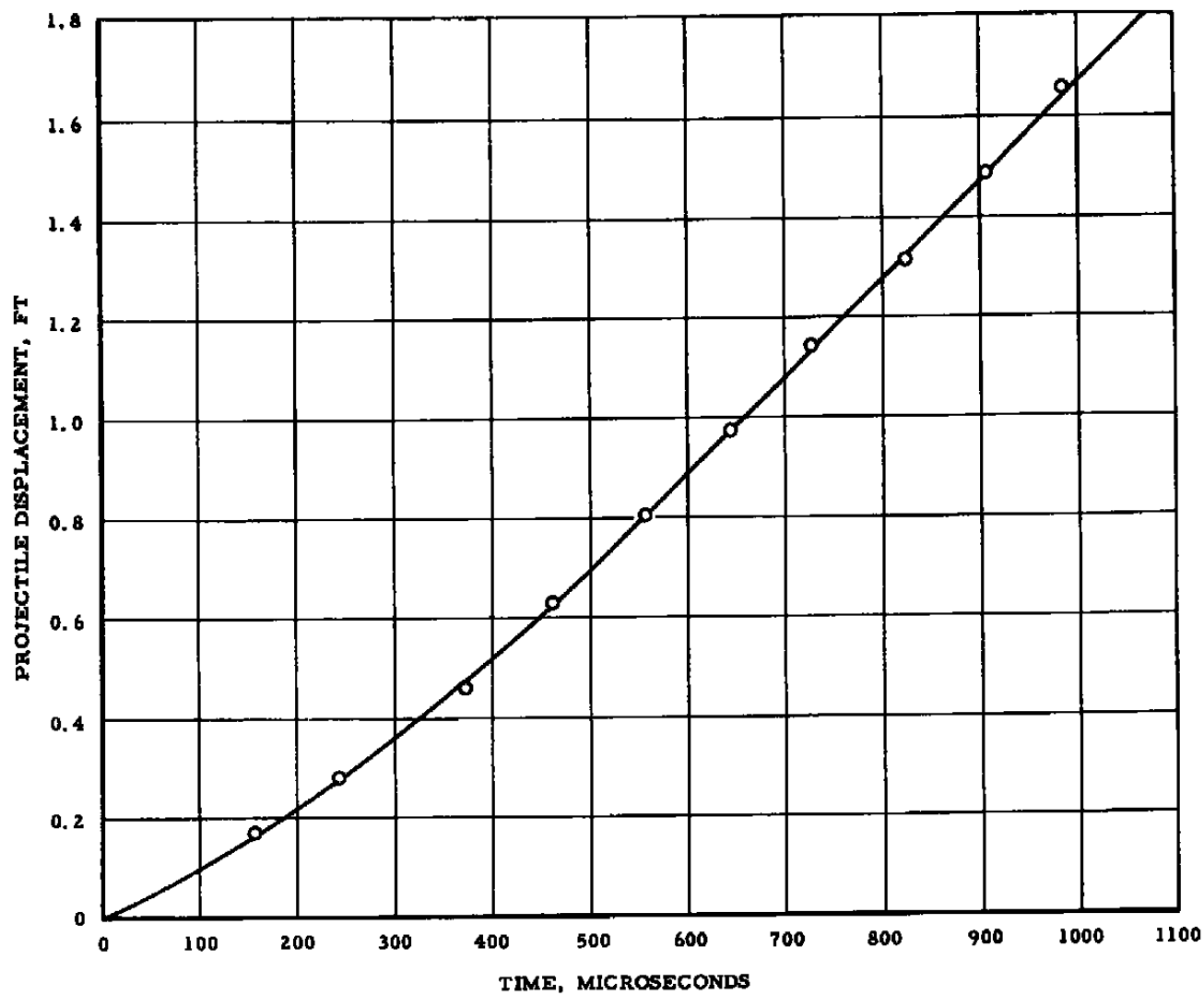Fig. 33 Microwave Reflectometer Recording

Fig. 34 Projectile Displacement Versus Time

AEDC-TR-61-9   *UNCLASSIFIED*

Arnold Engineering Development Center, ARO, Inc.,
Arnold Air Force Station, Tennessee
DEVELOPMENT OF HYPERVELOCITY RANGE TECH-
NIQUES AT ARNOLD ENGINEERING DEVELOPMENT
CENTER by J. Lukasiewicz, W. B. Stephenson, P. L.
Clemens, and D. E. Anderson, June 1961. 74 pp. (AEDC-
TR-61-9) (Contract No. AF 40(600)-800 S/A 11(60-110)).
                              Unclassified

22 references

Development of a hypervelocity launcher and range instru-
mentation in preparation for operation of a 1000-ft aero-
ballistic facility is described. A method has been evolved
for the gas-dynamics design of two-stage, light gas launch-
ers. Performance, limitations, and mechanical design
features of such launchers are discussed. Instrumentation
developments include: 1) projectile radiation actuated
detector and spark trigger, 2) simple, Fresnel-lens
shadowgraph performing satisfactorily at projectile speeds
                                          (over)

1. Hypervelocity guns
2. Light-gas guns
3. Aeroballistics ranges
4. Instrumentation--
     Development
I. Lukasiewicz, J
II. Stephenson, W B
III. Clemens, P. L.
IV. Anderson, D E.

UNCLASSIFIED

AEDC-TR-61-9   *UNCLASSIFIED*

Arnold Engineering Development Center, ARO, Inc.,
Arnold Air Force Station, Tennessee
DEVELOPMENT OF HYPERVELOCITY RANGE TECH-
NIQUES AT ARNOLD ENGINEERING DEVELOPMENT
CENTER by J Lukasiewicz, W B Stephenson, P. L.
Clemens, and D E. Anderson, June 1961. 74 pp. (AEDC-
TR-61-9) (Contract No. AF 40(600)-800 S/A 11(60-110)).
                              Unclassified

22 references

Development of a hypervelocity launcher and range instru
mentation in preparation for operation of a 1000-ft aero-
ballistic facility is described. A method has been evolved
for the gas-dynamics design of two-stage, light gas launch-
ers. Performance, limitations, and mechanical design
features of such launchers are discussed Instrumentation
developments include: 1) projectile radiation actuated
detector and spark trigger, 2) simple, Fresnel-lens
shadowgraph performing satisfactorily at projectile speeds
                                          (over)

1. Hypervelocity guns
2 Light-gas guns
3 Aeroballistics ranges
4. Instrumentation--
     Development
I. Lukasiewicz, J.
II Stephenson, W B
III. Clemens, P L.
IV. Anderson, D. E.

UNCLASSIFIED

AEDC-TR-61-9   *UNCLASSIFIED*

Arnold Engineering Development Center, ARO, Inc.,
Arnold Air Force Station, Tennessee
DEVELOPMENT OF HYPERVELOCITY RANGE TECH-
NIQUES AT ARNOLD ENGINEERING DEVELOPMENT
CENTER by J. Lukasiewicz, W. B. Stephenson, P. L
Clemens, and D E. Anderson, June 1961. 74 pp. (AEDC-
TR 61-9) (Contract No. AF 40(600)-800 S/A 11(60-110)).
                              Unclassified

22 references

Development of a hypervelocity launcher and range instru-
mentation in preparation for operation of a 1000-ft aero-
ballistic facility is described. A method has been evolved
for the gas-dynamics design of two-stage, light gas launch-
ers. Performance, limitations, and mechanical design
features of such launchers are discussed Instrumentation
developments include: 1) projectile radiation actuated
detector and spark trigger, 2) simple, Fresnel-lens
shadowgraph performing satisfactorily at projectile speeds
                                          (over)

1 Hypervelocity guns
2. Light-gas guns
3 Aeroballistics ranges
4. Instrumentation--
     Development
I. Lukasiewicz, J.
II Stephenson, W. B.
III. Clemens, P. L.
IV. Anderson, D E.

UNCLASSIFIED

AEDC-TR-61-9   *UNCLASSIFIED*

Arnold Engineering Development Center, ARO, Inc.,
Arnold Air Force Station, Tennessee
DEVELOPMENT OF HYPERVELOCITY RANGE TECH-
NIQUES AT ARNOLD ENGINEERING DEVELOPMENT
CENTER by J. Lukasiewicz, W. B. Stephenson, P. L.
Clemens, and D. E. Anderson, June 1961. 74 pp. (AEDC-
TR-61-9) (Contract No AF 40(600)-800 S/A 11(60-110)).
                              Unclassified

22 references

Development of a hypervelocity launcher and range instru-
mentation in preparation for operation of a 1000-ft aero-
ballistic facility is described. A method has been evolved
for the gas-dynamics design of two-stage, light gas launch-
ers. Performance, limitations, and mechanical design
features of such launchers are discussed. Instrumentation
developments include: 1) projectile radiation actuated
detector and spark trigger, 2) simple, Fresnel-lens
shadowgraph performing satisfactorily at projectile speeds
                                          (over)

1. Hypervelocity guns
2. Light-gas guns
3. Aeroballistics ranges
4. Instrumentation--
     Development
I Lukasiewicz, J.
II Stephenson, W B.
III. Clemens, P L.
IV. Anderson, D. E.

UNCLASSIFIED

AEDC-TR-61-9

of 26,000 ft/sec, 3) telemeter capable of transmitting
model pressure measurements at launch accelerations of
200,000 g, 4) microwave velocity measuring technique.

AEDC-TR-61-9

of 26,000 ft/sec, 3) telemeter capable of transmitting
model pressure measurements at launch accelerations of
200,000 g, 4) microwave velocity measuring technique.

AEDC-TR-61-9

of 26,000 ft/sec, 3) telemeter capable of transmitting
model pressure measurements at launch accelerations of
200,000 g, 4) microwave velocity measuring technique.

AEDC-TR-61-9

of 26,000 ft/sec, 3) telemeter capable of transmitting
model pressure measurements at launch accelerations of
200,000 g, 4) microwave velocity measuring technique.

Cut on broken line

AEDC-TR-61-9

UNCLASSIFIED

Arnold Engineering Development Center, ARO, Inc.,
Arnold Air Force Station, Tennessee
DEVELOPMENT OF HYPERVELOCITY RANGE TECH-
NIQUES AT ARNOLD ENGINEERING DEVELOPMENT
CENTER by J. Lukasiewicz, W. B. Stephenson, P. L.
Clemens, and D. E. Anderson, June 1961. 74 pp. (AEDC
TR-61-9) (Contract No. AF 40(600) 800 S/A 11(60-110)).
Unclassified

22 references

Development of a hypervelocity launcher and range instru-
mentation in preparation for operation of a 1000-ft aero-
ballistic facility is described. A method has been evolved
for the gas-dynamics design of two-stage, light gas launch-
ers. Performance, limitations, and mechanical design
features of such launchers are discussed. Instrumentation
developments include: 1) projectile radiation actuated
detector and spark trigger, 2) simple, Fresnel-lens
shadowgraph performing satisfactorily at projectile speeds
(over)

1. Hypervelocity guns
2. Light-gas guns
3. Aeroballistics ranges
4. Instrumentation--
   Development
I. Lukasiewicz, J.
II. Stephenson, W. B
III. Clemens, P. L.
IV. Anderson, D. E.

UNCLASSIFIED

AEDC-TR-61-9

UNCLASSIFIED

Arnold Engineering Development Center, ARO, Inc.,
Arnold Air Force Station, Tennessee
DEVELOPMENT OF HYPERVELOCITY RANGE TECH-
NIQUES AT ARNOLD ENGINEERING DEVELOPMENT
CENTER by J. Lukasiewicz, W. B. Stephenson, P L.
Clemens, and D. E. Anderson, June 1961. 74 pp. (AEDC-
TR-61-9) (Contract No AF 40(600)-800 S/A 11(60-110)).
Unclassified

22 references

Development of a hypervelocity launcher and range instru-
mentation in preparation for operation of a 1000-ft aero-
ballistic facility is described. A method has been evolved
for the gas-dynamics design of two-stage, light gas launch-
ers. Performance, limitations, and mechanical design
features of such launchers are discussed. Instrumentation
developments include: 1) projectile radiation actuated
detector and spark trigger, 2) simple, Fresnel-lens
shadowgraph performing satisfactorily at projectile speeds
(over)

1. Hypervelocity guns
2. Light-gas guns
3. Aeroballistics ranges
4. Instrumentation--
   Development
I. Lukasiewicz, J
II. Stephenson, W B
III. Clemens, P. L.
IV. Anderson, D. E.

UNCLASSIFIED

AEDC-TR-61-9

UNCLASSIFIED

Arnold Engineering Development Center, ARO, Inc.,
Arnold Air Force Station, Tennessee
DEVELOPMENT OF HYPERVELOCITY RANGE TECH-
NIQUES AT ARNOLD ENGINEERING DEVELOPMENT
CENTER by J. Lukasiewicz, W. B. Stephenson, P. L.
Clemens, and D. E. Anderson, June 1961. 74 pp (AEDC-
TR-61-9) (Contract No. AF 40(600)-800 S/A 11(60-110))
Unclassified

22 references

Development of a hypervelocity launcher and range instru-
mentation in preparation for operation of a 1000-ft aero-
ballistic facility is described. A method has been evolved
for the gas-dynamics design of two-stage, light gas launch-
ers. Performance, limitations, and mechanical design
features of such launchers are discussed. Instrumentation
developments include: 1) projectile radiation actuated
detector and spark trigger, 2) simple, Fresnel-lens
shadowgraph performing satisfactorily at projectile speeds
(over)

1 Hypervelocity guns
2. Light-gas guns
3. Aeroballistics ranges
4 Instrumentation--
   Development
I. Lukasiewicz, J.
II Stephenson, W B
III Clemens, P. L.
IV Anderson, D. E.

UNCLASSIFIED

AEDC-TR-61-9

UNCLASSIFIED

Arnold Engineering Development Center, ARO, Inc.,
Arnold Air Force Station, Tennessee
DEVELOPMENT OF HYPERVELOCITY RANGE TECH-
NIQUES AT ARNOLD ENGINEERING DEVELOPMENT
CENTER by J. Lukasiewicz, W. B. Stephenson, P. L.
Clemens, and D. E. Anderson, June 1961. 74 pp. (AEDC-
TR-61-9) (Contract No. AF 40(600)-800 S/A 11(60-110))
Unclassified

22 references

Development of a hypervelocity launcher and range instru-
mentation in preparation for operation of a 1000-ft aero-
ballistic facility is described. A method has been evolved
for the gas-dynamics design of two-stage, light gas launch-
ers. Performance, limitations, and mechanical design
features of such launchers are discussed. Instrumentation
developments include 1) projectile radiation actuated
detector and spark trigger, 2) simple, Fresnel-lens
shadowgraph performing satisfactorily at projectile speeds
(over)

1. Hypervelocity guns
2. Light-gas guns
3. Aeroballistics ranges
4. Instrumentation--
   Development
I. Lukasiewicz, J.
II Stephenson, W. B.
III. Clemens, P. L.
IV. Anderson, D. E.

UNCLASSIFIED

AEDC-TR-61-9

of 26,000 ft/sec, 3) telemeter capable of transmitting model pressure measurements at launch accelerations of 200,000 g, 4) microwave velocity measuring technique.